

# 1 **Estimating the depth and evolution of intrusions at resurgent** 2 **calderas: Los Humeros (Mexico)**

3 Stefano Urbani<sup>1</sup>, Guido Giordano<sup>1,2</sup>, Federico Lucci<sup>1</sup>, Federico Rossetti<sup>1</sup>, Valerio Acocella<sup>1</sup>,  
4 Gerardo Carrasco- Núñez<sup>3</sup>

5 <sup>1</sup>Dipartimento di Scienze, Università degli Studi Roma Tre, L.go S.L. Murialdo 1, I-00146 Rome, Italy

6 <sup>2</sup>CNR - IDPA c/o Università degli Studi di Milano, Via Luigi Mangiagalli, 34, 20133 Milano

7 <sup>3</sup>Centro de Geociencias, Universidad Nacional Autónoma de México, Campus UNAM Juriquilla, 76100, Queretaro,  
8 Mexico

9 *Correspondence to:* Stefano Urbani (stefano.urban@uniroma3.it)

10 **Abstract.** Resurgent calderas are excellent targets for geothermal exploration, as they are associated with the shallow  
11 emplacement of magma, resulting in widespread and long lasting hydrothermal activity. Resurgence is classically  
12 attributed to the uplift of a block or dome resulting from the inflation of the collapse-forming magma chamber due to  
13 the intrusion of new magma. The Los Humeros volcanic complex (LHVC; Mexico), consists of two nested calderas: the  
14 outer and older Los Humeros formed at 164 ka and the inner, Los Potreros, formed at 69ka. The latter is resurgent and  
15 currently the site of an active and exploited geothermal field (63MWe installed). Here we aim at better defining the  
16 characteristics of the resurgence in Los Potreros, by integrating field work with analogue models, evaluating the spatio-  
17 temporal evolution of the deformation and the depth and extent of the intrusions responsible for the resurgence which  
18 may represent also the local heat source(s).

19 Structural field analysis and geological mapping show that Los Potreros caldera floor is characterized by several lava  
20 domes and cryptodomes (with normal faulting at the top) that suggest multiple deformation sources localized in narrow  
21 areas.

22 The analogue experiments simulate the deformation pattern observed in the field, consisting of magma intrusions  
23 pushing a domed area developing an apical depression. To define the possible depth of the intrusion responsible for the  
24 observed surface deformations, we apply tested relations for elliptical sources to our experiments with sub-circular  
25 sources. We found that these relations are independent of the source and surface dome eccentricity and suggest that the  
26 magmatic sources inducing the deformation in Los Potreros are located at very shallow depths (hundreds of meters),  
27 which is in agreement with the well data and field observations. We propose that the recent deformation at LHVC is not  
28 a classical resurgence associated with the bulk inflation of a deep magma reservoir; rather this is related to the ascent of  
29 shallow (<1 km) multiple magma bodies. A similar multiple source model of the subsurface structure has been also  
30 proposed for other calderas with an active geothermal system (Usu volcano, Japan) suggesting that the model proposed  
31 may have wider applicability.

## 32 **1 Introduction**

33 Caldera resurgence consists of the post-collapse uplift of part of the caldera floor. Resurgence has been described in  
34 several calderas worldwide (Smith and Bailey, 1968; Elston, 1984; Lipman, 1984 and references therein), representing a  
35 frequent step in caldera evolution. Several mechanisms that trigger resurgence have been invoked, including the  
36 pressurization of the hydrothermal system (Moretti et al., 2018), regional earthquakes (Walter et al., 2009), and  
37 magmatic intrusion (Kennedy et al. 2012). Discriminating the contributions to the observed uplift of each of these  
38 mechanisms is often challenging (Acocella, 2014). However, despite the possible hydrothermal and tectonic

39 contributions, field observations in eroded resurgent calderas (e.g. Tomochic, Swanson and McDowell, 1985; Kutcharo,  
40 Goto and McPhie 2018; Turkey Creek, Du Bray and Pallister, 1999) coupled with the long timescale of the uplift of the  
41 caldera floor (from tens to thousands years), suggest that the intrusion of magmatic bodies is the prevalent mechanism  
42 for resurgence.

43 Resurgence is commonly attributed to the emplacement of silicic magmas at different depth levels under limited  
44 viscosity contrasts with regard to the previously emplaced magma (Marsh, 1984; Galetto et al., 2017). However, though  
45 rare, resurgence may be also triggered by the injection of more primitive magma (Morán-Zenteno et al., 2004; Kennedy  
46 et al., 2012) or by the emplacement of basaltic sills, as recently documented at the Alcedo caldera (Galapagos; Galetto  
47 et al., 2019). The shape of the intracaldera resurgent structures is variable, being characterized by elliptical domes with  
48 longitudinal graben(s) at the top (e.g. Toba; De Silva et al., 2015; Snowdonia, Beavon, 1980; Timber Mountain,  
49 Christiansen et al., 1977) or, less commonly, by sub-circular domes (e.g. Cerro Galan, Folkes et al., 2011; Long Valley,  
50 Hildreth et al., 2017; Grizzly Peak, Fridrich et al., 1991) with both longitudinal grabens (Long Valley) or concentric  
51 fault blocks (Grizzly Peak) at their top.

52 Whatever is the shape, resurgence is often associated with hydrothermal and ore forming processes, since the circulation  
53 pattern and temperature gradients of geothermal fluids are structurally-controlled by the space-time distribution of faults  
54 and fractures and by the depth and shape of the magmatic sources (e.g. Guillou Frottier et al., 2000; Prinbow et al.,  
55 2003; Stix et al., 2003; Mueller et al., 2009; Giordano et al., 2014). Therefore, the characterisation of the magma that  
56 drives resurgence (location, depth and size) and of the factors controlling the release of heat (permeability, fracture  
57 patterns, and fluid flow) have important implications for the exploration and exploitation of renewable geothermal  
58 energy resources. In particular, the estimation of the location, depth and geometry of the magmatic sources is crucial to  
59 define the geothermal and mineral potential of resurgent calderas, allowing an economically sustainable exploration and  
60 exploitation of their resulted natural resources.

61 The depth and size of the magmatic sources influence the deformation style of the resurgence at the surface (Acocella et  
62 al., 2001). Deep sources (i.e. depth/diameter ratio  $\sim 1$  assuming a spherical source) are associated to resurgent blocks  
63 (e.g. Ischia and Pantelleria, Acocella and Funicello, 1999; Catalano et al., 2009), whereas shallower sources (i.e.  
64 depth/diameter ratio  $\sim 0.4$ ) to resurgent domes (e.g. Valles and Yenkahe, Kennedy et al., 2012; Brothelande et al., 2016).  
65 Moreover, uplift rates may change by one order of magnitude from  $\sim 1$  to  $\sim 10$  cm per year (e.g. Yellowstone and Iwo  
66 Jima, Chang et al., 2007; Ueda et al., 2018). Nevertheless, despite showing different uplift styles and rates, these natural  
67 examples share a common feature that is a coherent uplift of the caldera floor. A different style of deformation is  
68 observed at calderas characterized by the widespread and delocalized uplift of several minor portions of the caldera  
69 floor, associated with the shallow emplacement of sills and cryptodomes, as observed at Usu volcano (Japan,  
70 Matsumoto and Nakagawa, 2010; Tomya et al., 2010). Such deformation pattern suggests different depth(s) and  
71 extent(s) of the magma source(s). A better assessment of the subsurface structure in this type of calderas has crucial  
72 implications for geothermal exploration.

73 The Los Humeros Volcanic Complex (LHVC, Mexico) is an important geothermal target area, consisting of two nested  
74 calderas: Los Humeros (the outer, larger and older one; 164 ka) and Los Potreros (the inner, smaller and younger one;  
75 69 ka) (Fig. 1). The latter is characterized by the resurgence of its floor, interpreted to be due to the inflation of the  
76 magma chamber responsible for the collapse, with its top at ca 5 km depth (Norini et al., 2015, 2019).

77 This paper aims at (1) evaluating the depth of the intrusion(s) inducing the uplift in the LHVC area; (2) explain the  
78 spatio-temporal evolution of the observed deformation of the caldera floor and (3) test the validity of the linear  
79 relationship between the surface deformation structures and depth of elliptical sources (Brothelande and Merle 2015)

80 for sub-circular sources. To achieve these goals, we integrate results from structural field investigations carried out  
81 within the Los Potreros caldera with those derived from analogue experiments specifically designed to constrain the  
82 depth of the deformation source(s) in volcanic caldera environments. The obtained results show that: (1) the relation  
83 between the source depth and surface deformation structures is independent of the source eccentricity; (2) the LHVC is  
84 characterized by discontinuous and small-scale (areal extent  $\sim 1 \text{ km}^2$ ) surface deformations generated from multiple and  
85 shallow-emplaced ( $< 1 \text{ km}$  depth) magmatic bodies. These results should be taken into account for the planning of  
86 future geothermal operations at the LHVC and in other calderas showing similar surface deformation.

## 87 **2 Geological-structural setting**

88 LHVC is located at the eastern termination of the Trans Mexican Volcanic Belt (TMVB, see inset in Fig. 1). The TMVB  
89 is the largest Neogene volcanic arc in Mexico ( $\sim 1000 \text{ km}$  long and up to  $\sim 300 \text{ km}$  wide), commonly associated with the  
90 subduction of the Cocos and Rivera plates beneath the North American plate along the Middle American trench (Ferrari  
91 et al., 2012, and references therein). The LHVC consists of two nested calderas formed during the Pleistocene: the outer  
92  $18 \times 16 \text{ km}$  Los Humeros caldera and the inner  $10 \times 8 \text{ km}$  Los Potreros caldera (Fig. 1, Ferriz and Mahood, 1984;  
93 Norini et al., 2015; Carrasco-Núñez et al., 2017b).

94 Based on updated stratigraphic and geochronological information, the evolution of the LHVC can be divided into three  
95 main eruptive stages (Table 1, Carrasco-Núñez et al., 2017b, 2018). Pre-caldera volcanism extended between ca. 700  
96 and 164 ka (U-Th and  $^{39}\text{Ar}/^{40}\text{Ar}$  datings in Carrasco-Núñez et al., 2018), showing evidence for an extended building  
97 phase leading to the establishment of the large volume rhyolitic reservoir, which fed several lava domes erupted to the  
98 western border of the Los Humeros Caldera. A Caldera stage started at ca. 164 ka (U-Th and  $^{39}\text{Ar}/^{40}\text{Ar}$  ages, Carrasco-  
99 Núñez et al., 2018), with the eruption of the  $>115 \text{ km}^3$  (dense rock equivalent volume) Xaltipan ignimbrite that  
100 triggered the collapse of the Los Humeros caldera. This was followed by a Plinian eruptive episodic sequence,  
101 characterized by the emplacement of several rhyodacitic pumice fallout layers grouped as the Faby Tuff (Ferriz and  
102 Mahood, 1984). The Caldera stage ended with the eruption of the  $15 \text{ km}^3$  (dense rock equivalent volume) Zaragoza  
103 rhyodacite-andesite ignimbrite at  $69 \pm 16 \text{ ka}$  ( $^{39}\text{Ar}/^{40}\text{Ar}$  ages, Carrasco-Núñez et al., 2018) associated with the collapse of  
104 the nested Los Potreros caldera.

105 A post-caldera stage ( $< 69 \text{ ka}$ ) is interpreted by Carrasco-Núñez et al. (2018) as composed by two main eruptive phases:  
106 (i) a late Pleistocene resurgent phase, characterized by the emplacement of silica-rich small domes and disperse  
107 explosive activity within Los Potreros caldera, followed by (ii) Holocene basaltic to trachytic monogenetic volcanism  
108 both inside and at the caldera-rim. This eruptive behaviour indicates a change in the configuration of the magmatic  
109 plumbing system compared to the caldera stage of Los Humeros, when a single, large and homogenized magma  
110 reservoir was in existence (e.g. Ferriz and Mohood, 1984; Verma, 1985). Volcanological and petrological data indicate  
111 that the post-caldera volcanism is associated with a heterogeneous multi-layered system vertically distributed within the  
112 crust, with a deep (ca. 30 km depth) basaltic reservoir feeding progressively shallower and smaller distinct stagnation  
113 layers, pockets and batches up to very shallow conditions (ca. 3km) (Lucci et al., 2020), in agreement with recent  
114 conceptual models for magma reservoirs under caldera systems (e.g. Cashman and Giordano, 2014).

115 During the early resurgent phase of the post-caldera stage, rhyolitic domes were emplaced along the northern rim and  
116 within the Los Humeros caldera. Available ages span between  $44.8 \pm 1.7 \text{ ka}$  (U-Th ages) and  $50.7 \pm 4.4 \text{ ka}$  ( $^{39}\text{Ar}/^{40}\text{Ar}$   
117 ages), (Carrasco-Núñez et al., 2018). This effusive activity was followed by several explosive eruptions, which  
118 originated a dacitic air fall called Xoxoctic Tuff ( $0.6 \text{ km}^3$ , Ferriz and Mahood, 1984) and a pyroclastic sequence that

119 includes an explosive breccia and pyroclastic flow deposits comprising the Llano Tuff (Ferriz and Mahood 1984;  
120 Willcox, 2011).

121 The Holocene ring-fractures fed bimodal magmatism characterized by both explosive and effusive activity, producing  
122 several lava flows and domes, as well as the ca. 7 ka (C-14 age, Dávila-Harris and Carrasco-Núñez, 2014) Cuicuiltic  
123 Member during periods of dominant explosive activity. The Cuicuiltic Member consists of alternating pumices and  
124 scoriae erupted during contemporaneous sub-Plinian to Strombolian activity from multiple vents located mostly along  
125 the inner part of the caldera and outer caldera ring faults (Dávila-Harris and Carrasco-Núñez, 2014). During this phase,  
126 less evolved lavas (trachyandesite to basalt) were erupted within and outside the Los Potreros caldera, including the  
127 olivine-bearing basaltic lava that fills the previously formed Xalapasco crater (Fig. 1). Trachytic lava flows are the most  
128 recent products in the area, with an age of ca. 2.8 ka (C-14 age, Carrasco-Núñez et al., 2017b).

129 The reconstruction of the shallow stratigraphy within the Los Potreros caldera is chiefly derived from the analysis of  
130 available well-logs (Figs. 2a-b Carrasco-Núñez et al., 2017a, b). Overall, the post-caldera units are lithologically  
131 dominated by lava flows resting on ignimbrite deposits emplaced during the caldera stage. Ignimbrites of the caldera  
132 stage rest in turn on a thick sequence dominated by andesite lavas dated at ca. 1.4-2.8 Ma ( $^{39}\text{Ar}/^{40}\text{Ar}$  ages, Carrasco-  
133 Núñez et al., 2017a). The subsurface geometry of the pre- and syn-caldera products is shown in Figs. 2a-b, where the in-  
134 depth geometry of the different magmatic products are cross-correlated and projected along the N-S and E-W direction,  
135 respectively. The N-S projection shows a constant depth of the top surface of the pre-caldera andesites that is associated  
136 with a highly variable depth (down to -400 m) of the top surface of the syn-caldera Xaltipan ignimbrite. The W-E  
137 projection shows a higher depth variability of both the top surface of the pre-caldera group (down to -500 m between H-  
138 19 and H-25 wells) and that of the Xaltipan ignimbrite (down to -400 m between H-19 and H-10 wells). Basaltic and  
139 rhyolitic-dacitic lavas occur at various depths (Carrasco-Núñez et al., 2017a); rhyolites-dacites are located mostly at the  
140 base (H-20 and H-26 wells) or within (H-05 well) the caldera group or the old andesite sequence (H-25 and H-19  
141 wells). Basalts are located only within the pre-caldera andesite sequence, both at its base (in contact with the limestone  
142 basement; H-5 and H-8 wells) and at its top (in contact with the base of the caldera sequence; H-10 well). These  
143 bimodal lava products, showing an irregular lateral distribution, have been interpreted as subaerial (Carrasco-Núñez et  
144 al., 2017a).

145 The structural architecture of the LHVC is controlled by a network of active extensional fault systems, made of NNW-  
146 SSE, N-S, NE-SW and E-W striking fault strands cutting across the Los Potreros caldera floor. The following main  
147 faults were recognised (Norini et al., 2015, 2019; Calcagno et al., 2018) (Fig.1): (i) Maxtaloya (NNW-SSE striking), (ii)  
148 Los Humeros and Loma Blanca (N-S striking), (iii) Arroyo Grande (NE-SW striking), (iv) Las Viboras and Las Papas  
149 (E-W striking). Such active fault systems are interpreted as due to the recent/active resurgence of the Los Potreros  
150 Caldera. Since the faults do not show continuity beyond the caldera border, their scarps decrease in height towards the  
151 periphery of the caldera and the dip-slip displacement vectors show a semi-radial pattern (Norini et al., 2015).

152 The source of the areal uplift has been inferred to be the inflation of a saucer or cup shaped deep magmatic source  
153 elongated NNW-SSE, up warping a 8 x 4 km resurgent block, centred in the SE portion of the caldera, delimited to the  
154 W by the NNW-SSE main faults, and toward the north, east and south by the caldera rim (Fig.1, Norini et al., 2015,  
155 2019).

156 The seismic activity between 1994-2017 is clustered along the Loma Blanca, Los Humeros and Arroyo Grande faults  
157 (Lermo et al., 2018; Fig. 1). Most of the earthquakes show a magnitude ( $M_w$ ) between 1 and 2.5 and have been mainly  
158 interpreted as induced by the geothermal exploitation activity (injection of fluids and hydrofracturing; Lermo et al.,  
159 2018). Four major earthquakes ( $M_w$ = 3.2, 3.6, 3.9 and 4.2, at a depth of 1, 4, 2.2 and 1.8 km, respectively) have also

160 been reported, with focal depths close to the trace of the active faults (Loma Blanca and Los Humeros, Fig.1). Such  
161 major earthquakes have been interpreted as triggered by fault reactivation due to fluid/brine circulation injected from  
162 geothermal wells (Lermo et al., 2018).

### 163 **3 Methods**

164 This study is based on structural field work combined with analogue models aimed at constraining the depth of the  
165 deformation sources in the caldera domain. We also tested if the relation that constrains the depth of the source  
166 deformation from surface parameters adopting elliptical sources (Brothelande and Merle 2015) is verified also for sub-  
167 circular sources.

#### 168 **3.1 Structural field work**

169 Structural field work was carried out on the post-caldera (Late Pleistocene to Holocene) deposits to characterise the  
170 surface deformation related to the recent activity of the Los Potreros caldera and constrain the morphotectonic  
171 fingerprints of the resurgence to evaluate its source and areal extent. The geometry and distribution of the observable  
172 faults and joints were defined at the outcrop scale by measuring their attitudes (strike and dip; right-hand rule) and  
173 spacing. Fault kinematics was assessed through classical criteria on slickensides fault surfaces, such as Riedel shears,  
174 growth fibres and sheltering trails (Doblas, 1998). The published geological map (Carrasco-Núñez et al., 2017b) and  
175 geothermal well data have been used (Carrasco-Núñez et al., 2017a) to correlate the surface structures at a broader  
176 scale. The relationships between faulting and alteration have been assessed (e.g. Giordano et al. 2013; Vignaroli et al.  
177 2013, 2015)

#### 179 **3.2 Analogue models: experimental set-up and scaling**

180 Five experiments were undertaken to simulate the ascent of a viscous sub-circular intrusion in a brittle overburden to  
181 test the validity of existing relationships between the depth of elliptical intrusions and the observed surface deformation  
182 (Brothelande and Merle, 2015). The experimental set-up (Fig. 3) consists of a  $31 \times 31$  cm glass box filled with a sand  
183 pack (crust analogue) of variable thickness ( $T$ , of 10, 30 and 50 mm, respectively). In each experiment we imposed a  
184 layering using a non-cohesive marine sand below a layer of crushed silica sand (grain size = 40-200  $\mu\text{m}$ , cohesion = 300  
185 Pa), fixing the thickness ratio of the two layers ( $T_u/T_1$ ) to 1, to simulate the stratigraphy in Los Potreros (stiffer post  
186 caldera lava flows above softer and less cohesive ignimbrite deposits emplaced during the caldera collapse stage). At  
187 the base of the sand pack, a piston, controlled by a motor, pushes upward the silicone (magma analogue) placed inside a  
188 cylinder 8 cm in diameter. The injection rate is fixed for all the experiments to 2 mm/hr and each experiment was  
189 stopped at the onset of the silicone extrusion. Both sand and silicone physical properties are listed in Table 2.

190 At the end of each experiment, the surface has been covered with sand to preserve their final topography and was  
191 wetted with water for cutting in sections to appreciate the subsurface deformation. Such sections were used to measure  
192 the mean dip of the apical depression faults ( $\theta$ ) induced by the rising silicone. A digital camera monitored the top view  
193 deformation of each experiment at 0.02 fps and a laser scanner, placed next to the camera, provided high-resolution data  
194 (maximum error  $\pm 0.5$  mm) of the vertical displacement to measure in detail the geometrical features of the deformation  
195 i.e. dome diameter ( $L_d$ ), apical depression width ( $L_g$ ) and dome flank mean dip ( $\alpha$ ). According to the Buckingham-II  
196 theorem (Merle and Borgia 1996 and references therein), our models need 7 independent dimensionless numbers to be  
197 properly scaled (i.e. 10 variables minus three dimensions; Table 2). Such dimensionless numbers can be defined as the  
198 ratios ( $\Pi$ ) listed in Table 3. Some values of  $\Pi_5$ , representing the ratio between the inertial and viscous forces, are very

199 small both in nature and experiments ( $1.3 \times 10^{-20}$  and  $6.1 \times 10^{-10}$ , respectively), indicating that the inertial forces are  
200 negligible compared to the viscous forces in both cases.

## 201 **4 Results**

### 202 **4.1 Structural geology**

203 The outcropping post-caldera lithologies within the Los Potreros Caldera consist of: (1) the Cuicuiltic Member, which  
204 blankets most of the surface of the upper half of the studied area; (2) basaltic lava flows filling the Xalapasco crater and  
205 the NW portion of the caldera; and (3) trachyandesitic and trachytic lava domes and thick flows extending in the  
206 southern half of the caldera and rhyolitic domes in its central part (Fig. 4). Field work documented that the more  
207 evolved lavas form five nearly N-S trending elliptical domes, distributed in both sides of the Los Humeros Fault (Figs. 4  
208 and 5a): (i) a 2 km long  $\times$  1.2 km wide trachytic dome located to the west of the Maxtaloya and Los Humeros faults, (ii)  
209 a 1  $\times$  0.7 km trachyandesitic dome located in a northeast area of the Maxtaloya fault, and (iii) one trachyandesitic and  
210 two obsidian smaller domes (0.4  $\times$  0.2 km) to the eastern side of the Los Humeros Fault (LH-11 in Fig. 4).

211 Field work concentrated on the three main uplifted areas corresponding to the surface expression of the Loma Blanca,  
212 Arroyo Grande and Los Humeros faults (labelled LH1-2, LH9 and LH10 respectively in Fig. 4). The observed  
213 structures in these uplifted areas (joints and faults) affect the deposits of the post-caldera phase. Based on field  
214 evidence, we also propose a revised interpretation of the surface structures identified by previous studies (Norini et al.,  
215 2015, 2019), distinguishing between lineaments (morphological linear scarps, with no measurable fault offsets and/or  
216 alteration at the outcrop scale), active and inactive faults, instead associated with measurable fault offsets and with  
217 active or fossil alteration, respectively (Fig. 4). We present below a description of the structures mapped in the studied  
218 area, highlighting their temporal and spatial relationships with the post-caldera geological formations. We identified two  
219 inactive faults (Maxtaloya and Arroyo Grande), a morphological lineament (Las Papas) and two currently active faults  
220 (Los Humeros and Loma Blanca).

#### 221 **4.1.1 Las Papas lineament (sites LH-07, LH-08)**

222 The E-W trending Las Papas lineament is localised within the Cuicuiltic Member (LH-07; Fig. 5b). We identified an  
223 erosional surface along the scarp, where unaltered and undeformed Cuicuiltic Member rocks rest above the Xoxotic  
224 Tuff (LH-08, Fig. 5c). The E-W trending morphological lineament of Las Papas is probably due to differential erosion  
225 of the softer layers of the pyroclastic deposits, successively blanketed by the Cuicuiltic Member.

#### 226 **4.1.2 Arroyo Grande (site LH-09) and Maxtaloya scarps**

227 The NE-SW Arroyo Grande scarp (Fig. 6a) exposes strongly altered and faulted (NW striking faults, mean attitude  
228 N144°/68°, number of data ( $n$ ) = 8) lavas and ignimbrites unconformably covered by the unaltered Cuicuiltic Member  
229 (Fig.6b). The offset observed at the outcrop-scale for the single fault strands is ca. 0.5 m, with a dominant normal dip-  
230 slip kinematics (pitch angle of the slickenlines ranging 99°-106°). The inferred cumulative displacement at Arroyo  
231 Grande is  $\sim$  10 m. Similarly, an outcrop on the Maxtaloya scarp (in front of well H-6) shows altered trachyandesites  
232 covered by unaltered Cuicuiltic Member rocks (Fig. 6c).

#### 233 **4.1.3 Los Humeros (site LH-10)**

234 The fault scarp of the N-S striking (mean attitude  $N174^{\circ}/73^{\circ}$ ,  $n=8$ ) Los Humeros Fault exposes the altered portions of  
235 the Cuicuiltic Member. Fault population analysis reveals a dominant normal dip-slip (mean pitch angle of the  
236 slickenlines:  $84^{\circ}$ ) kinematics, as documented by both Riedel shears and carbonate-quartz growth steps. The main fault  
237 surface is sutured by a trachyandesitic extrusion (Fig. 6d), localised along an aligned N-S dome (site LH-11 in Fig. 4).  
238 Moreover,  $\sim 150$  m southward from the outcrop of the fault scarp, a  $5 \times 3$  m wide trachyandesitic plug shows vertical  
239 striation on its surface due to a subsurface vertical flow of the trachyandesite (Fig. 6e). The observed displacement at  
240 the outcrop scale, as indicated by the height of the fault scarp, is  $\sim 10$  m.

#### 241 **4.1.4 Loma Blanca (LH-01, LH-02)**

242 The Loma Blanca Fault system (sites LH-01 and LH-02) is located in an active degassing area, where faults and  
243 fractures are frequent. The fault system is on top of an elongated crest (within an apical depression) of a morphological  
244 bulge,  $\sim 1$  km in width and 30 m in height. At this location, the Cuicuiltic Member and the underlying trachyandesite  
245 lavas are strongly altered (Fig. 6f). Evidence of stockwork veining and diffuse fracturing of the lavas suggests  
246 hydrofracturing and structurally controlled fluid flow and alteration. A set of NNE-SSW striking conjugate extensional  
247 faulting and jointing (joint spacing  $\sim 0.5$  m) is observed. The faults (mean attitude  $N26^{\circ}/71^{\circ}$ ,  $n=6$ ) show normal dip-slip  
248 kinematics (pitch of the slickenlines ranging  $82^{\circ}$ - $104^{\circ}$ ). Joint systems found in the Cuicuiltic Member strike sub-parallel  
249 to the faults (mean attitude  $N37^{\circ}/72^{\circ}$ ,  $n=14$ ). The inferred cumulative displacement of the faults, estimated by the depth  
250 of the apical depression, is  $\sim 5$  m.

251 In summary, the 22 mapped faults in all the structural outcrops of the area show a main NNW-SSE strike (Fig. 6g) with  
252 a dominant dip slip movement (mean pitch angle of slickenlines  $88^{\circ}$ ,  $n=16$ ) which is sub-parallel to the N-S elongation  
253 of the lava domes and the Xalapasco crater.

#### 254 **4.2 Experimental results**

255 Here we show three representative experiments with increasing overburden thickness (experiments 1-3-5 with  $T=10$ ,  
256  $30$  and  $50$  mm). Table 4 shows the measured parameters in the experiments. Some experiments (1-2 and 3-4) were  
257 replicated with the same imposed boundary conditions and show the same result (i.e. apical depression width and dome  
258 diameter), which ensures model reproducibility (Fig. 8 and Fig. S1).

259 Overall, the experiments show a similar deformation pattern: a first stage characterized by the uplift of a sub-circular  
260 dome, bordered by inward dipping reverse faults, and a second stage characterized by the subsidence of the apical part  
261 of the dome where normal faulting occurs (apical depression formation Fig. 7a-i). The reverse and normal faults are ring  
262 faults and are associated with the formation of radial fractures from the dome centre. A different shape of the apical  
263 depression is observed with  $T/D > 0.12$ . In exp.1 ( $T/D = 0.12$ ) an annular peripheral depression formed as the silicone  
264 reached the surface at the edge of the cylinder (Fig. 7c). Conversely, in exp. 3 and 5 ( $T/D=0.37$  and  $0.63$  respectively) a  
265 sub-circular apical depression formed as the silicone reached the surface at the centre of the dome (Fig. 7g, m).

266 Despite the  $T/D$  ratio, all the experiments show that both the dome diameter and apical depression width increase  
267 linearly with the overburden thickness (ranging from  $105$  to  $164$  mm and  $14$  to  $58$  mm respectively, Table 4, Fig. 8). The  
268 dome diameter increases abruptly with time, becoming almost constant at an early stage of the experiment (Fig. 9a); the  
269 apical depression width shows a similar pattern even if it enlarges slightly with time (after the first abrupt increase) as  
270 the silicone rises towards the surface (Fig. 9b), suggesting that the intrusion depth has a higher influence on the apical  
271 depression width, in agreement with Brothelande and Merle (2015).

272

## 273 **5. Discussion**

### 274 **5.1 Interpretation of the analogue experiments**

275 The deformation pattern observed in the analogue experiments for thicker overburdens (experiments 3-4 and 5 with  
276  $T/D= 0.37$  and  $0.63$ ), showing a sub-circular dome and an apical depression, is in agreement with previous analogue  
277 experimental results (Acocella et al., 2001; Marti et al. 1994; Walter and Troll 2001). However, for thinner overburdens  
278 (exps. 1-2,  $T/D= 0.12$ ), we observed a new deformation pattern at the surface consisting of an annular peripheral  
279 depression due to the rising of the silicone at the edge of the cylinder rather than its centre. We infer that in these  
280 experiments, since the rising silicone was very close to the surface, the sagging of the sand overburden pushed  
281 downward the centre of the silicone that squeezed up at the edges of the cylinder. Such process may also explain the  
282 two linear grabens that formed in the experiments with elliptical sources for small overburden thicknesses (ratio  $T/D \sim$   
283  $0.1$ , Brothelande and Merle 2015).

284 The deformation pattern observed in our experiments is independent of the imposed strain (i.e. uplift) rate or the  
285 viscosity of the intruding material as suggested by the similarity with results obtained in previous studies with higher  
286 strain rates (Acocella and Mulugeta, 2002) or lower viscosity intruding materials (Galletto et al., 2017; Marti et al. 1994;  
287 Walter and Troll, 2001). On the other hand, the occurrence of an apical depression is dependent on the thickness (i.e.  
288 depth) of the intrusion since thin intrusions relative to their depths will generate sub-circular domes without any apical  
289 depression (Galland et al., 2009; Galland, 2012). Moreover, our results confirm that the apical depression width shows a  
290 linear correlation with the source depth (Fig. 8) as estimated in Brothelande and Merle (2015) for elongated sources.  
291 This evidence documents that such relation is independent of the source eccentricity or shape of the extensional  
292 structures at the top of the dome (i.e. linear graben or sub-circular depression) suggesting that any elongation of the  
293 surface structure represents only a minor complication of the basic deformation pattern as already pointed out by  
294 (Roche et al., 2000).

295

### 296 **5.2 Origin and extent of the resurgence in the LHVC**

297 The distribution of alteration patterns and deformation characteristics of the post-caldera deposits can be used to infer  
298 the origin and extent of the uplift within the Los Potreros resurgent caldera. The extent of the local deformation and  
299 alteration of the ubiquitous 7.4 ka Cuicuiltic Member, which blankets the caldera floor, allow constraining the spatio-  
300 temporal evolution of the surficial deformation and associated uplifts in Los Potreros. Unaltered and undeformed  
301 deposits of the Cuicuiltic Member crop out along the E-W Las Papas lineament and unconformably cover altered and  
302 faulted lavas and ignimbrites along the Arroyo Grande and Maxtaloya scarps. Alteration and deformation of the  
303 Cuicuiltic Member occur along the Los Humeros Fault scarp and within the apical depression of the Loma Blanca  
304 bulge. The vertical striations of the trachyandesitic plug near the Los Humeros fault scarp suggest that the ascent of the  
305 plug induced the uplift, the normal dip-slip faulting and alteration of the Cuicuiltic Member.

306 The observations suggest that Los Potreros is not a classic resurgent caldera (i.e. a caldera characterised by a large-scale  
307 process localized in a single area) but is characterised by uplift pulses discontinuous in space and time, inducing small-  
308 scale deformations at each pulse (Fig. 10a-d). In particular, it was active in the south and north-eastern sector of the  
309 caldera, at Maxtaloya and Arroyo Grande (Fig. 10a), prior to the deposition of the Cuicuiltic Member ( $\sim 7.4$  ka), and  
310 then shifted towards N along the Los Humeros and Loma Blanca scarps during and post the eruption of the Cuicuiltic  
311 Member (Fig. 10b-d). The felsic lava found at the Los Humeros Fault scarp shows a similar mineral assemblage to the  
312 felsic domes located further south (Fig. 4); thus, the Los Humeros scarp may represent the final stage (i.e. effusive  
313 eruption of felsic magmas, (Fig. 10c) of the uplift process, which is thus driven by the ascent of relatively narrow



314 (hundreds of meters) and highly viscous felsic magma batches. This is supported by the N-S elongation of the identified  
315 lava domes which is sub-parallel to the orientation of the measured fault planes (NNW-SSE), indicating that the  
316 observed deformation is closely related to the post-caldera volcanism. The emplacement of such magma bodies is  
317 inferred here to drive the recent uplift and deformation of the Loma Blanca bulge, as suggested by the active fumaroles  
318 and extensive alteration of both the Cuicuiltic Member and post-caldera lavas (Fig. 10d). The recent emplacement of  
319 shallow magma bodies should be considered as a possible scenario for the interpretation of the seismicity in Los  
320 Potreros, which have been so far interpreted as induced by geothermal exploitation (Lermo et al., 2018). In fact, the  
321 highest magnitude of the recent seismicity reached between 3.2 and 4.2 and may well be consistent with a volcano-  
322 tectonic origin due to shallow magma emplacement, more than induced by reinjection of hydrothermal fluids (cf. Evans  
323 et al., 2012 and references therein).

324 To further support the above interpretation from field observations, results from the presented analogue models were  
325 used to constrain the magma source depth from the geometrical parameters measured in the experiments ( $L_g$ ,  $\theta$ ,  $\alpha$ , Table  
326 4). We calculated the theoretical overburden thickness (i.e. the intrusion depth,  $T_t$ , Table 4) as follow (Brothelande and  
327 Merle, 2015):

$$328 \quad T_t = \frac{1}{2} L_g \times \frac{\sin(\theta + \alpha)}{\cos \theta} \quad (1)$$

329 Comparing the percentage difference ( $\sigma$ ) between the imposed experimental ( $T$ ) and theoretical ( $T_t$ ) overburden  
330 thickness values, we calculate the associated error in the evaluation of the intrusion depth in the models ( $\sigma$ , Table 4,  
331 Fig.8). We then use equation (1) for the evaluation of the heat source depth at the Loma Blanca bulge considering  $\sigma \sim$   
332 40 % (maximum value of the experiments excluding those showing an annular depression that was not observed in the  
333 field). For the Loma Blanca bulge  $L_g = 286$  m,  $\theta = 71^\circ$ ,  $\alpha = 4.5^\circ$ , the estimated intrusion depth is  $425 \pm 170$  m. Such  
334 relatively shallow depth is within the range of depths of rhyolitic-dacitic bodies drilled in geothermal wells (spanning  
335 from -300 to -1700 m, Fig. 2a-b) and is consistent with the hypothesis that the uplift is driven by small and delocalized  
336 magmatic intrusions, as suggested by the field data. These rhyolites-dacites bodies have been previously interpreted as  
337 subaerial in origin (Carrasco-Núñez et al., 2017a), but we suggest that at least some of them can be reinterpreted as  
338 intrusions of felsic cryptodomes based on the following considerations: (i) the occurrence of rhyolite-dacite lava bodies  
339 within the thick pre-caldera old andesite sequence is unusual and does not have a subaerial counterpart; (ii) the rhyolite  
340 body in well H-20 (Fig. 2b) up warps both the intracaldera ignimbrite sequence and the post-caldera lavas (showing a  
341 reduced thickness) indicating that the caldera forming ignimbrites do not levelled out the paleo-topography, as it should  
342 be expected; and (iii) the top of the Xaltipan ignimbrite shows a higher depth variation than the pre caldera andesite  
343 (Fig. 2a) highlighting a local and discontinuous uplifting of the Xaltipan ignimbrite. Such evidence can be more easily  
344 reconciled with the intrusion of felsic cryptodomes within the volcanic sequence.

345

### 346 **5.3 Implications for the structure of the LHVC geothermal field**

347 The combination of field and modelling data support that the uplift in Los Potreros caldera is due to multiple  
348 deformation sources in narrow areas that do not represent resurgence *sensu stricto*. Such localized recent deformation  
349 within Los Potreros caldera appears to be linked to small magmatic intrusions located at relatively shallow depths (i.e. <  
350 1 km) as in Loma Blanca, where the estimated intrusion depth calculated from the experimental data is  $425 \pm 170$  m.

351 This model differs from the generally accepted idea of a resurgence in Los Potreros induced by the inflation of a saucer  
352 or cup shaped deep magmatic intrusion (Norini et al., 2015, 2019), which may be active at a larger scale but does not  
353 explain the highly discontinuous deformation and alteration patterns with pulses scattered along the caldera floor.

354 Neither the thermal anomalies identified by Norini et al. (2015) fit well with the classic resurgence as temperatures are

355 unexpectedly cold beneath the centre of the inferred resurgent block, where the highest temperatures should be  
356 expected. By contrast, sharp and narrow temperature peaks, spatially coincident with Los Humeros and Loma Blanca  
357 faults, are consistent with the presence of shallow and delocalized heat sources. Indeed, the inflation of the deep magma  
358 chamber of the LHVC, inferred to be at 5 to 7-8 km of depth (Verma, 1983, 2000, 2011) and extending 9 km in radius  
359 and 6 km in length (thus coinciding with the Los Humeros caldera rim, Verma et al., 1990), should have induced a much  
360 wider uplift and with higher magnitude than the one observed in the field. Resurgence resulting from magma  
361 remobilization of the deep chamber that produced collapse is characterized by a larger-scale surface deformation  
362 (thousands of meters of uplift extending for tens of kilometres on the surface) as shown in many large calderas  
363 worldwide (Toba, de Silva et al., 2015; Cerro Galan, Folkes et al., 2011; Ischia, Carlino, 2012, Selva et al. 2019).  
364 It is therefore unlikely that the replenishment of new magma in the caldera forming deep magma chamber accounts for  
365 the magnitude (few tens of meters) and discontinuous spatial distribution of the deformation in Los Potreros.  
366 Such a model of the recent uplifting in Los Potreros is supported by field-based petrographic-mineralogical analysis  
367 showing that the present-day magmatic plumbing system is characterized by multiple magma levels spanning from a  
368 deep (30-33 km) basaltic reservoir to very shallow (~ 1.5 km), smaller, trachyandesitic-trachytic magma batches (Lucci  
369 et al., 2020).  
370 A similar model of the plumbing system has been proposed to explain the eruptive activity of Usu volcano (Japan) since  
371 1663, a post caldera cone of the Toya caldera consisting of a basaltic main edifice surmounted by three felsic lava  
372 domes and more than ten cryptodomes. Petrochemical data at Usu suggest the presence of multiple magma batches (i.e.  
373 sills) at 0.25-2 km deep that originated from partial melting of a metagabbro (Matsumoto and Nakagawa, 2010; Tomya  
374 et al., 2010).  
375 Our proposed model has implications for planning future geothermal exploration: siting of future geothermal wells  
376 should consider that the presence of shallow heat sources within the caldera might complicate the pattern of isotherms  
377 associated with the deeper heat flow.

## 378 **6 Conclusions**

379 By integrating field work with analogue models, we constrain the Late Pleistocene-Holocene spatio-temporal evolution  
380 of volcanism of the LHVC and estimate the depth of the magmatic intrusions feeding the active geothermal system.  
381 New findings on experimental analogue models of resurgent domes are also provided.

382 These are the main results that can be extracted from this study:

- 383 1. The distribution of the alteration patterns and deformation of the Cuicuiltic Member suggests that the recent (post-  
384 caldera collapse) uplift in Los Potreros caldera moved progressively northwards, from the south and north-eastern  
385 sector of the caldera towards N along the Los Humeros and Loma Blanca scarps.
- 386 2. The estimated depth of the intrusions responsible for such uplift is very shallow, as calculated from the experimental  
387 data for the Loma Blanca bulge ( $425 \pm 170$  m).
- 388 3. The recent uplift in Los Potreros is discontinuous in space and time, inducing small-scale (areal extent ~ 1 km<sup>2</sup>)  
389 deformations originating from multiple and shallow (< 1 km depth) magmatic bodies, thus not representing a classic  
390 resurgent caldera, which usually involves large-scale deformation (areal extent of several km<sup>2</sup>).
- 391 4. The relationship between the depth of the magmatic source and the surface parameters of resurgent domes is  
392 independent of the source eccentricity, similarly to what already verified for sub-circular intrusions.

393

## 394 **Acknowledgements**

395 CFE is kindly acknowledged for allowing work on the Los Humeros geothermal field. Federico Galetto helped for laser  
396 scanner data processing. Fabio Corbi and Matteo Trolese provided technical support in building the experimental set-up.  
397 Gianluca Norini is acknowledged for logistic support in the field. Alessandra Pensa kindly helped with figure drawings.  
398 Funded by the European Union's Horizon 2020 GEMex Project (grant agreement No. 727550) and by the Mexican  
399 Energy Sustainability Fund CONACYT-SENER, WP 4.5 of the Project 2015-04-268074. More information can be  
400 found on the GEMex Website: <http://www.gemex-h2020.eu>. The Grant to Department of Science, Roma Tre University  
401 (MIUR-Italy Dipartimenti di Eccellenza, ARTICOLO 1, COMMI 314 – 337 LEGGE 232/2016) is gratefully  
402 acknowledged.

403

#### 404 **References**

405 Acocella, V.: Great challenges in volcanology: how does the volcano factory work?, *Front. Earth Sci.*, 2:4,  
406 <https://doi.org/10.3389/feart.2014.00004>, 2014.

407 Acocella, V., and Funicello, R.: The interaction between regional and local tectonics during resurgent doming: the case  
408 of the island of Ischia, Italy, *J. Volcanol. Geoth. Res.*, 88, 109-123, [https://doi.org/10.1016/S0377-0273\(98\)00109-7](https://doi.org/10.1016/S0377-0273(98)00109-7),  
409 1999.

410 Acocella, V., and Mulugeta, G.: Experiments simulating surface deformation induced by pluton emplacement,  
411 *Tectonophysics*, 352, 275-293, [https://doi.org/10.1016/S0040-1951\(02\)00218-4](https://doi.org/10.1016/S0040-1951(02)00218-4), 2002.

412 Acocella, V., Cifelli, F., and Funicello, R.: The control of overburden thickness on resurgent domes, *J. Volcanol. Geoth.*  
413 *Res.*, 111, 137–153, [https://doi.org/10.1016/S0377-0273\(01\)00224-4](https://doi.org/10.1016/S0377-0273(01)00224-4), 2001.

414 Arellano, V.M., García, A., Barragán, R.M., Izquierdo, G., Aragón, A., and Nieva, D.: An updated conceptual model of  
415 the Los Humeros geothermal reservoir (Mexico), *J. Volcanol. Geoth. Res.*, 124, 67–88, [https://doi.org/10.1016/S0377-  
416 0273\(03\)00045-3](https://doi.org/10.1016/S0377-0273(03)00045-3), 2003.

417 Beavon, R.V.: A resurgent cauldron in the early Paleozoic of Wales, U.K., *J. Volcanol. Geoth. Res.*, 7, 157-174,  
418 [https://doi.org/10.1016/0377-0273\(80\)90025-6](https://doi.org/10.1016/0377-0273(80)90025-6), 1980.

419 Brothelande, E., Peltier, A., Got, J.L., Merle, O., Lardy, M., and Garaebiti, E.: Constraints on the source of resurgent  
420 doming inferred from analogue and numerical modeling — Implications on the current feeding system of the Yenkahe  
421 dome–Yasur volcano complex (Vanuatu), *J. Volcanol. Geoth. Res.*, 322, 225–240,  
422 <https://doi.org/10.1016/j.jvolgeores.2015.11.023>, 2016.

423 Brothelande, E., and Merle, O.: Estimation of magma depth for resurgent domes: An experimental approach, *Earth*  
424 *Planet. Sc. Lett.*, 412, 143–151, <https://doi.org/10.1016/j.epsl.2014.12.011>, 2015.

425 Calcagno, P., Evanno, G., Trumpy, E., Carlos Gutiérrez-Negrín, L., Macías, J.L., Carrasco-Núñez, G., and Liotta, D.:  
426 Preliminary 3-D geological models of Los Humeros and Acoculco geothermal fields (Mexico)-H2020 GEMex Project,  
427 *Adv. Geosci.*, 45, 321–333, <https://doi.org/10.5194/adgeo-45-321-2018>, 2018.

428 Carlino, S.: The process of resurgence for Ischia Island (southern Italy) since 55 ka: The laccolith model and  
429 implications for eruption forecasting, *B. Volcanol.*, 74, 947–961. <https://doi.org/10.1007/s00445-012-0578-0>, 2012.

430 Carrasco-Núñez, G., and Branney, M.J.: Progressive assembly of a massive layer of ignimbrite with a normal-to-reverse  
431 compositional zoning: The Zaragoza ignimbrite of central Mexico, *B. Volcanol.*, 68, 3–20,  
432 <https://doi.org/10.1007/s00445-005-0416-8>, 2005.

433 Carrasco-Núñez, G., McCurry, M., Branney, M.J., Norry, M., and Willcox, C.: Complex magma mixing, mingling, and  
434 withdrawal associated with an intra-Plinian ignimbrite eruption at a large silicic caldera volcano: Los Humeros of  
435 central Mexico, *Bull. Geol. Soc. Am.*, 124, 1793–1809, <https://doi.org/10.1130/B30501.1>, 2012.

436 Carrasco-Núñez, G., López-Martínez, M., Hernández, J., and Vargas, V.: Subsurface stratigraphy and its correlation  
437 with the surficial geology at Los Humeros geothermal field, eastern Trans-Mexican Volcanic Belt, *Geothermics*, 67, 1–  
438 17, <https://doi.org/10.1016/j.geothermics.2017.01.001>, 2017a.

439 Carrasco-Núñez, G., Hernández, J., De León, L., Dávila, P., Norini, G., Bernal, J.P., Jicha, B., Navarro, M., López-  
440 Quiroz, P., and Digitalis, T.: Geologic Map of Los Humeros volcanic complex and geothermal field, eastern Trans-  
441 Mexican Volcanic Belt, *Terra Digitalis*, 1, 1–11, <https://doi.org/10.22201/igg.terradigitalis.2017.2.24.78>, 2017b.

442 Carrasco-Núñez, G., Bernal, J.P., Dávila, P., Jicha, B., Giordano, G., and Hernández, J.: Reappraisal of Los Humeros  
443 volcanic complex by new U/Th zircon and <sup>40</sup>Ar/<sup>39</sup>Ar dating: Implications for greater geothermal potential, *Geochem.*  
444 *Geophys. Geosy.*, 19, 132-149, <https://doi.org/10.1002/2017GC007044>, 2018.

445 Cashman, K. V., & Giordano, G.: Calderas and magma reservoirs, *J. Volcanol. Geoth. Res.*, 288, 28-45,  
446 <https://doi.org/10.1016/j.jvolgeores.2014.09.007>, 2014.

447 Catalano, S., De Guidi, G., Lanzafame, G., Monaco, C., and Tortotici, L.: Late quaternary deformation on the island on  
448 Pantelleria: new constraints for the recent tectonic evolution of the Sicily Channel Rift (southern Italy). *J. Geodyn.* 48,  
449 75–82, 2009.

450 Chang, W.L., Smith, R.B., Wicks, C., Farrell, J.M., and Puskas, C.M.: Accelerated uplift and magmatic intrusion of the  
451 Yellowstone Caldera, 2004 to 2006, *Science*, 318, 952-956, <https://doi.org/10.1126/science.1146842>, 2007.

452 Christiansen, R.L., Lipman, P.W., Carr, W.J., Byers, F.M., Orkild, P.P., and Sargent, K.A.: Timber Mountain-Oasis  
453 Valley caldera complex of southern Nevada, *Geol. Soc. Am. Bull.*, 88, 943-959, [https://doi.org/10.1130/0016-7606\(1977\)88<943:TMVCCO>2.0.CO;2](https://doi.org/10.1130/0016-7606(1977)88<943:TMVCCO>2.0.CO;2), 1977.

455 Dávila-Harris, P., and Carrasco-Núñez, G.: An unusual syn-eruptive bimodal eruption: The Holocene Cuicuiltic  
456 Member at Los Humeros caldera, Mexico, *J. Volcanol. Geoth. Res.*, 271, 24–42,  
457 <https://doi.org/10.1016/j.jvolgeores.2013.11.020>, 2014.

458 de Silva, S.L., Mucek, A.E., Gregg, P.M., and Pratomo, I.: Resurgent Toba - field, chronologic, and model constraints  
459 on time scales and mechanisms of resurgence at large calderas, *Front. Earth Sci.*, 3, 1–17,  
460 <https://doi.org/10.3389/feart.2015.00025>, 2015.

461 Doblás, M.: Slickenside kinematic indicators, *Tectonophysics*, 295, 187–197, [https://doi.org/10.1016/S0040-1951\(98\)00120-6](https://doi.org/10.1016/S0040-1951(98)00120-6), 1998.

463 Du Bray, E.A., and Pallister, J.S.: Recrystallization and anatexis along the plutonic–volcanic contact of the Turkey  
464 Creek caldera, Arizona, *Geol. Soc. Am. Bull.*, 111, 143–153, [https://doi.org/10.1130/0016-7606\(1999\)111<0143:RAAATP>2.3.CO;2](https://doi.org/10.1130/0016-7606(1999)111<0143:RAAATP>2.3.CO;2), 1999.

466 Elston, W.: Mid-Tertiary ash flow tuff cauldrons, southwestern New Mexico, *J. Geophys. Res.*, 89, 8733–8750,  
467 <https://doi.org/10.1029/JB089iB10p08733>, 1984.

468 Evans, K.F., Zappone, A., Kraft, T., Deichmann, N., and Moia, F.: A survey of the induced seismic responses to fluid  
469 injection in geothermal and CO<sub>2</sub> reservoirs in Europe, *Geothermics*, 41, 30-54,  
470 <https://doi.org/10.1016/j.geothermics.2011.08.002>, 2012.

471 Ferrari, L., Orozco-Esquivel, T., Manea, V., and Manea, M.: The dynamic history of the Trans-Mexican Volcanic Belt  
472 and the Mexico subduction zone, *Tectonophysics*, 522–523, 122–149, <https://doi.org/10.1016/j.tecto.2011.09.018>, 2012.

473 Ferriz, H., and Mahood, G.A.: Eruption Rates and Compositional Trends at Los Humeros Volcanic Center, Puebla,  
474 Mexico, *J. Geophys. Res.*, 89, 8511-8524, <https://doi.org/10.1029/JB089iB10p08511>, 1984.

475 Folkes, C.B., Wright, H.M., R.A.F. Cas, de Silva, S.L., Lesti, C., and Viramonte, J.G.: A re-appraisal of the stratigraphy  
476 and volcanology of the Cerro Galán volcanic system, NW Argentina, *B. Volcanol.*, 73, 1427–1454,  
477 <https://doi.org/10.1007/s00445-011-0459-y>, 2011.

478 Fridrich, C.J., Smith, R.P., DeWitt, E., McKee, E.H.: Structural, eruptive, and intrusive evolution of the Grizzly Peak  
479 caldera, Sawatch Range, Colorado, *Geol. Soc. Am. Bull.*, 103, 1160-1177, [https://doi.org/10.1130/0016-7606\(1991\)103<1160:SEAIEO>2.3.CO;2](https://doi.org/10.1130/0016-7606(1991)103<1160:SEAIEO>2.3.CO;2), 1991.

481 Galetto, F., Acocella, V., and Caricchi, L.: Caldera resurgence driven by magma viscosity contrasts, *Nat. Commun.*, 8,  
482 1–11, <https://doi.org/10.1038/s41467-017-01632-y>, 2017.

483 Galetto, F., Bagnardi, M., Acocella, V., and Hooper, A.: Noneruptive unrest at the caldera of Alcedo Volcano (Galápagos  
484 Islands) revealed by InSAR data and geodetic modelling, *J. Geophys. Res.*, 124, 3365–3381,  
485 <https://doi.org/10.1029/2018JB017103>, 2019.

486 Galland, O.: Experimental modelling of ground deformation associated with shallow magma intrusions, *Earth Planet.  
487 Sc. Lett.*, 317-318, 145-156, <https://doi.org/10.1016/j.epsl.2011.10.017>, 2012.

488 Galland, O., Planke, S., Ragnhild Neumann, E., and Malthé-Sørenssen, A.: Experimental modelling of shallow magma  
489 emplacement: Application to saucer-shaped intrusions, *Earth Planet. Sc. Lett.*, 277, 373-383,  
490 <https://doi.org/10.1016/j.epsl.2008.11.003>, 2009.

491 Giordano, G., Pinton, A., Cianfarra, P., Baez, W., Chiodi, A., Viramonte, J., Norini G., and GropPELLI, G.: Structural  
492 control on geothermal circulation in the Cerro Tuzgle–Tocomar geothermal volcanic area (Puna plateau, Argentina), *J.  
493 Volcanol. Geotherm. Res.*, 249, 77-94. <https://doi.org/10.1016/j.jvolgeores.2012.09.009>, 2013

494 Giordano, G., De Benedetti, A. A., Bonamico, A., Ramazzotti, P., and Mattei, M.: Incorporating surface indicators of  
495 reservoir permeability into reservoir volume calculations: Application to the Colli Albani caldera and the Central Italy  
496 Geothermal Province, *Earth-Sci. Rev.*, 128, 75-92, <https://doi.org/10.1016/j.earscirev.2013.10.010>, 2014.

497 Goto, Y., and McPhie, J.: Tectonics, structure, and resurgence of the largest Quaternary caldera in Japan: Kutcharo,  
498 Hokkaido, *Geol. Soc. Am. Bull.*, 130, 1307-1322, <https://doi.org/10.1130/B31900.1>, 2018.

499 Guillou-Frottier, L., Burov, E.B., and Milési, J.P.: Genetic links between ash-flow calderas and associated ore deposits  
500 as revealed by large-scale thermo-mechanical modelling, *J. Volcanol. Geoth. Res.*, 102, 339–361,  
501 [https://doi.org/10.1016/S0377-0273\(00\)00246-8](https://doi.org/10.1016/S0377-0273(00)00246-8), 2000.

502 Hildreth, W., Fierstein, J., and Calvert, A.: Early postcaldera rhyolite and structural resurgence at Long Valley  
503 Caldera, California, *J. Volcanol. Geoth. Res.*, 335, 1-34, <http://dx.doi.org/10.1016/j.jvolgeores.2017.01.005>, 2017.

504 Kennedy, B., Wilcock, J., and Stix, J.: Caldera resurgence during magma replenishment and rejuvenation at Valles and  
505 Lake City calderas, *B. Volcanol.*, 74, 1833–1847, <https://doi.org/10.1007/s00445-012-0641-x>, 2012.

506 Lipman, P. W.: The roots of ash flow calderas in Western North America: windows into the tops of granitic batholiths, *J.  
507 Geophys. Res.*, 89, 8801–8841, <https://doi.org/10.1029/JB089iB10p08801>, 1984.

508 Lermo, J., Lorenzo, C., Jiménez, N., Ramos, E., Ángulo, J., Israel, J., Téllez, N., Machado, O., Álvarez, I., Torres, R.,  
509 Alfaro R.: Analisis de la actividad sismica (1994-2016), su relacion con los pozos inyectoros y productores y aplicación  
510 de nuevas tecnicas geofisica para caracterizar las zonas anómalas del campo geotérmico de Los Humeros, CEMIE-  
511 GEO, Mexico, Internal Rep., 42 pp., 2018.

512 Lucci, F., Carrasco-Núñez, G., Rossetti, F., Theye, T., White, J. C., Urbani, S., Azizi, H., Asahara, Y., and Giordano, G.:  
513 Anatomy of the magmatic plumbing system of Los Humeros Caldera (Mexico): implications for geothermal systems,  
514 *Solid Earth Discuss.*, <https://doi.org/10.5194/se-2019-86>, 2020.

515 Marsh, B.D.: On the mechanics of caldera resurgence, *J. Geophys. Res.*, 89, 8245–8251,  
516 <https://doi.org/10.1029/JB089iB10p08245>, 1984.

517 Marti, J., Ablay, G.J., Redshaw, L.T., and Sparks, R.S.J.: Experimental studies of collapse calderas, *J. Geol. Soc.*  
518 London, 151, 919-929, <https://doi.org/10.1144/gsjgs.151.6.0919>, 1994.

519 Merle, O., Borgia, A.: Scaled experiments of volcanic spreading, *J. Geophys. Res.*, 101, 13805-13817,  
520 <https://doi.org/10.1029/95JB03736>, 1996.

521 Morán-Zenteno, D.J., Alba-Aldave, L.A., Solé, J., and Iriondo, A.: A major resurgent caldera in southern Mexico: the  
522 source of the late Eocene Tilzapotla ignimbrite. *J. Volcanol. Geoth. Res.*, 136, 97–119,  
523 <https://doi.org/10.1016/j.jvolgeores.2004.04.002>, 2004.

524 Moretti, R., Troise, C., Sarno, F., and De Natale, G.: Caldera unrest driven by CO<sub>2</sub> induced drying of the deep  
525 hydrothermal system, *Sci. Rep. UK*, 8, <https://doi.org/10.1038/s41598-018-26610-2>, 2018.

526 Mueller, W.U., Stix, J., Corcoran, P.L., Daigneault, R.: Subaqueous calderas in the Archean Abitibi greenstone belt: An  
527 overview and new ideas, *Ore Geol. Rev.*, 35, 4–46, <https://doi.org/10.1016/j.oregeorev.2008.12.003>, 2009.

528 Norini, G., Groppelli, G., Sulpizio, R., Carrasco-Núñez, G., Dávila-Harris, P., Pellicoli, C., Zucca, F., and De Franco,  
529 R.: Structural analysis and thermal remote sensing of the Los Humeros Volcanic Complex: Implications for volcano  
530 structure and geothermal exploration, *J. Volcanol. Geoth. Res.*, 301, 221–237,  
531 <https://doi.org/10.1016/j.jvolgeores.2015.05.014>, 2015.

532 Norini, G., Carrasco-Núñez, G., Corbo-Camargo, F., Lermo, J., Hernández Rojas, J., Castro, C., Bonini, M., Montanari,  
533 D., Corti, G., Moratti, G., Chavez, G., Ramirez, M., and Cedillo F.: The structural architecture of the Los Humeros  
534 volcanic complex and geothermal field, *J. Volcanol. Geoth. Res.*, 381, 312-329.  
535 <https://doi.org/10.1016/j.jvolgeores.2019.06.010>, 2019.

536 Matsumoto, A., and Nakagawa, M.: Formation and evolution of silicic magma plumbing system: Petrology of the  
537 volcanic rocks of Usu volcano, Hokkaido, Japan, *J. Volcanol. Geoth. Res.*, 196, 185–207,  
538 <https://doi.org/10.1016/j.jvolgeores.2010.07.014>, 2010.

539 Pribnow, D.F.C., Schütze, C., Hurter, S.J., Flechsig, C., Sass, J.H.: Fluid flow in the resurgent dome of Long Valley  
540 Caldera: Implications from thermal data and deep electrical sounding. *J. Volcanol. Geoth. Res.*, 127, 329–345,  
541 [https://doi.org/10.1016/S0377-0273\(03\)00175-6](https://doi.org/10.1016/S0377-0273(03)00175-6), 2003.

542 Roche, O., Druitt, T.H., and Merle, O.: Experimental study of caldera formation, *J. Geophys. Res.*, 105,  
543 <https://doi.org/10.1029/1999JB900298>, 395-416, 2000.

544 Selva, J., Acocella, V., Bisson, M., Caliro, S., Costa, A., Della Seta, M., P. De Martino, S. de Vita, C. Federico,  
545 G. Giordano, S. Martino, and C. Cardaci.: Multiple natural hazards at volcanic islands: a review for the Ischia volcano  
546 (Italy), *Journal of Applied Volcanology*, 8(1), 5., <https://doi.org/10.1186/s13617-019-0086-4>, 2019

547 Smith, R. L., and Bailey, R. A.: Resurgent cauldrons, *Geol. Soc. Am. Mem.*, 116, 613–662,  
548 <https://doi.org/10.1130/MEM116>, 1968.

549 Stix, J., Kennedy, B., Hannington, M., Gibson, H., Fiske, R., Mueller, W., Franklin, J.: Caldera-forming processes and  
550 the origin of submarine volcanogenic massive sulfide deposits, *Geology*, 31, 375–378, [https://doi.org/10.1130/0091-7613\(2003\)031<0375:CFPATO>2.0.CO;2](https://doi.org/10.1130/0091-7613(2003)031<0375:CFPATO>2.0.CO;2), 2003.

551  
552 Swanson, E., and McDowell, F.: Geology and geochronology of the Tomochic caldera, Chihuahua, Mexico, *Geol. Soc.*  
553 *Am. Bull.*, 96, 1477-1482, [https://doi.org/10.1130/0016-7606\(1985\)96<1477:GAGOTT>2.0.CO;2](https://doi.org/10.1130/0016-7606(1985)96<1477:GAGOTT>2.0.CO;2), 1985.

554 Tomiya, A., Takahashi, E., Furukawa, N., Suzuki, T.: Depth and evolution of a silicic magma chamber: Melting  
555 experiments on a low-K rhyolite from Usu volcano, Japan, *J. Petrol.*, 51, 1333–1354,  
556 <https://doi.org/10.1093/petrology/egg021>, 2010.

557 Ueda, H., Nagai, M., and Tanada, T.: Phreatic eruptions and deformation of Ioto Island (Iwo-jima), Japan, triggered by  
558 deep magma injection, *Earth Planets Space*, 70, <https://doi.org/10.1186/s40623-018-0811-y>, 2018.

559 Verma, M.P., Verma, S.P., and Sanvicente, H.: Temperature field simulation with stratification model of magma  
560 chamber under Los Humeros caldera, Puebla, Mexico, *Geothermics*, 19, 187–197, [https://doi.org/10.1016/0375-](https://doi.org/10.1016/0375-6505(90)90015-4)  
561 [6505\(90\)90015-4](https://doi.org/10.1016/0375-6505(90)90015-4), 1990.

562 Verma, S.P., Gómez-Arias, E., and Andaverde, J.: Thermal sensitivity analysis of emplacement of the magma chamber  
563 in Los Humeros caldera, Puebla, Mexico, *Int. Geol. Rev.*, 53, 905–925, <https://doi.org/10.1080/00206810903234296>,  
564 2011.

565 Verma, S.P.: Magma genesis and chamber processes at Los Humeros caldera, Mexico - Nd and Sr isotope data, *Nature*,  
566 302, 52–55, <https://doi.org/10.1038/302052a0>, 1983.

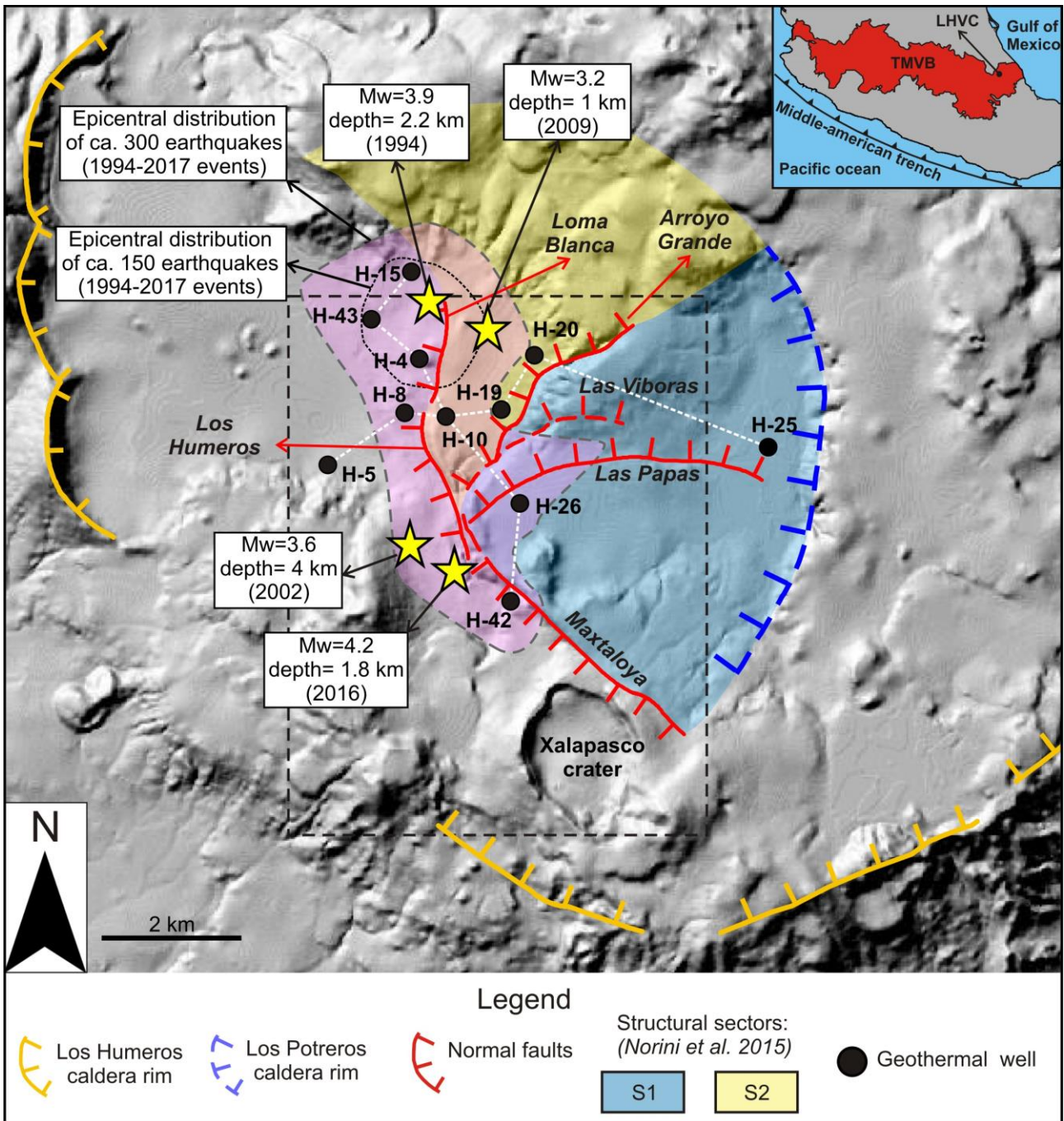
567 Verma, S.P.: Geochemical evidence for a lithospheric source for magmas from Los Humeros caldera, Puebla, Mexico.  
568 *Chem. Geol.* 164, 35–60, [https://doi.org/10.1016/S0009-2541\(99\)00138-2](https://doi.org/10.1016/S0009-2541(99)00138-2), 2000.

569 Vignaroli, G., Pinton, A., De Benedetti, A. A., Giordano, G., Rossetti, F., Soligo, M., and Berardi, G.: Structural  
570 compartmentalisation of a geothermal system, the Torre Alfina field (central Italy), *Tectonophysics*, 608, 482-498.  
571 <https://doi.org/10.1016/j.tecto.2013.08.040>, 2013. Vignaroli, G., Aldega, L., Balsamo, F., Billi, A., De Benedetti, A. A.,  
572 De Filippis, L., Giordano G. and Rossetti, F.: A way to hydrothermal paroxysm, Colli Albani volcano, Italy, *Geol. Soc.*  
573 *Am. Bull.*, 127(5-6), 672-687. <https://doi.org/10.1130/B31139.1>, 2015.

574 Walter, T.R., and Troll, V.R.: Formation of caldera periphery faults: an experimental study, *B. Volcanol.*, 63, 191-203,  
575 <https://doi.org/10.1007/s004450100135>, 2001. Walter, T.R., Wang, R., Acocella, V., Neri, M., Grosser, H., and Zschau, J:  
576 Simultaneous magma and gas eruptions at three volcanoes in southern Italy: an earthquake trigger ?, *Geology*, 37, 251–  
577 254, <https://doi.org/10.1130/G25396A>, 2009.

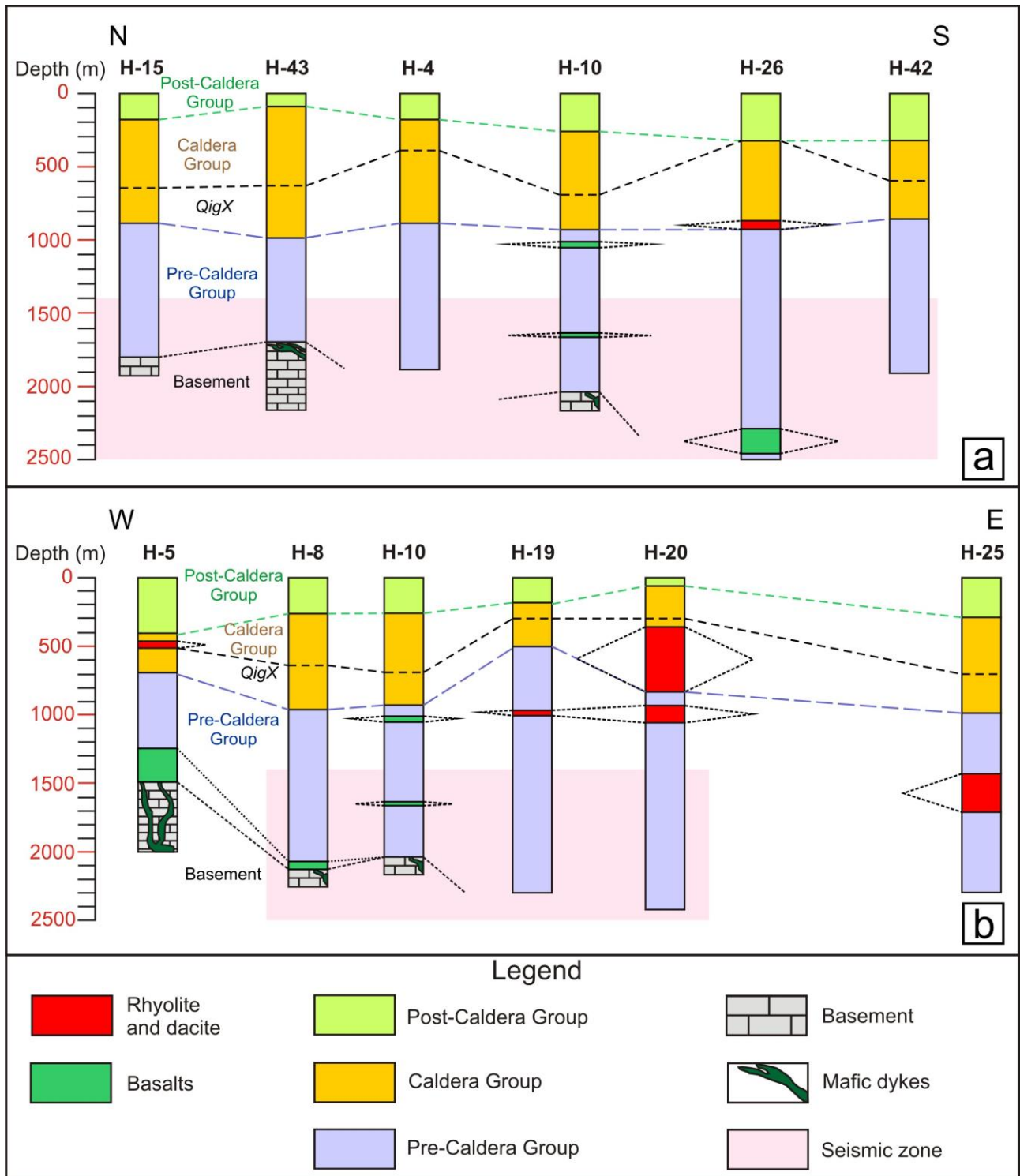
578 Wilcox, C.P.: Eruptive, magmatic and structural evolution of a large explosive caldera volcano, Los Humeros, Central  
579 Mexico, Ph.D. thesis, Department of Geology, University of Leicester, United Kingdom, 317 pp., 2011.





580  
 581 **Figure 1:** Shaded relief image (illuminated from the NE) obtained from 15 m resolution DEM of the Los Humeros Volcanic  
 582 Complex (LHVC) showing the main structural features (faults and caldera rim, modified from Norini et al. (2015); Calcagno  
 583 et al. (2018) and some geothermal wells referred in the text and in Figures 2a-b. The white dashed lines indicate the direction  
 584 of the correlation sections shown in Figures 2a-b. The black rectangle indicates the studied area within the Los Potreros  
 585 Caldera shown in Figure 4. The Inset box show the location of the LHVC (black dot and arrow) within the eastern sector of  
 586 the Trans Mexican Volcanic Belt (TMVB). The structural sectors S1 and S2 correspond to the resurgent block inferred by  
 587 Norini et al. (2015). Seismicity data from Lermo et al. (2018).  
 588  
 589  
 590  
 591  
 592





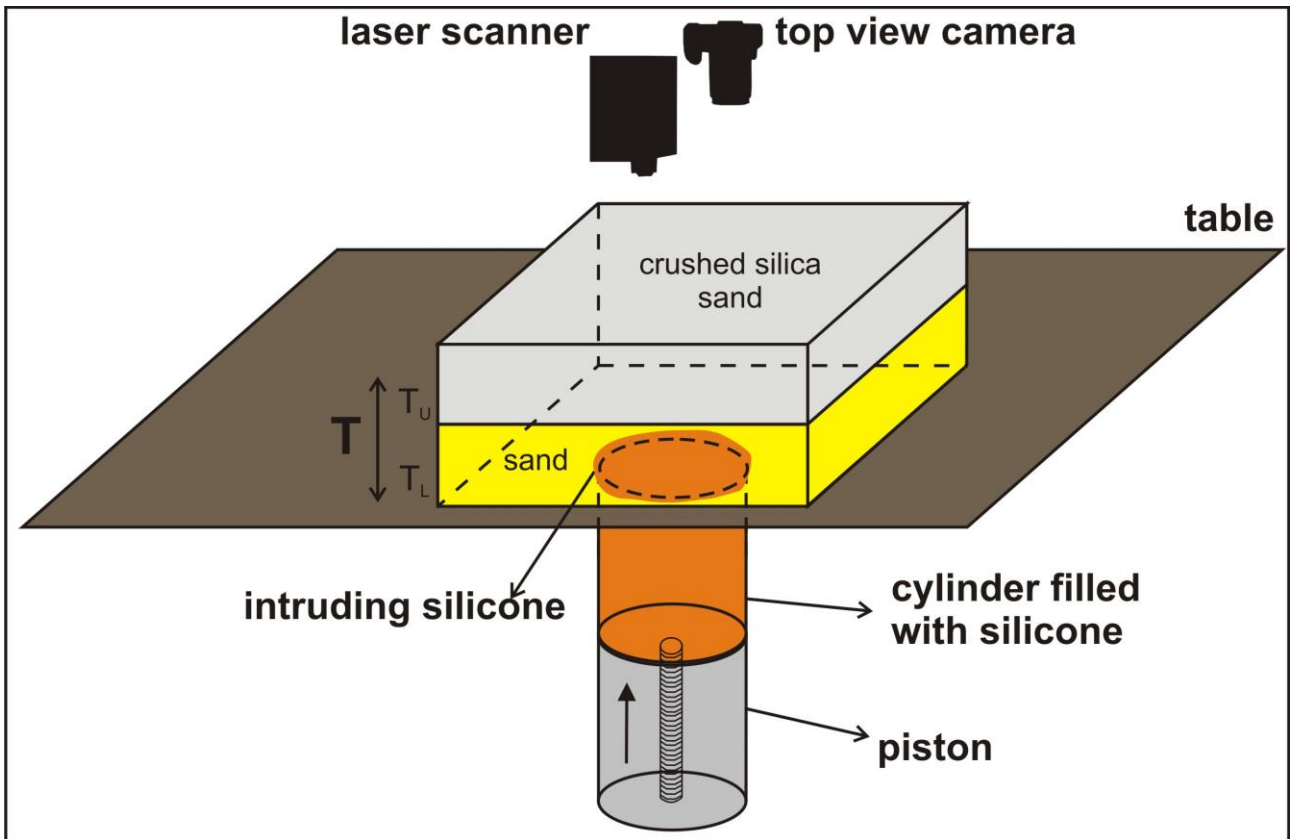
593

594

595

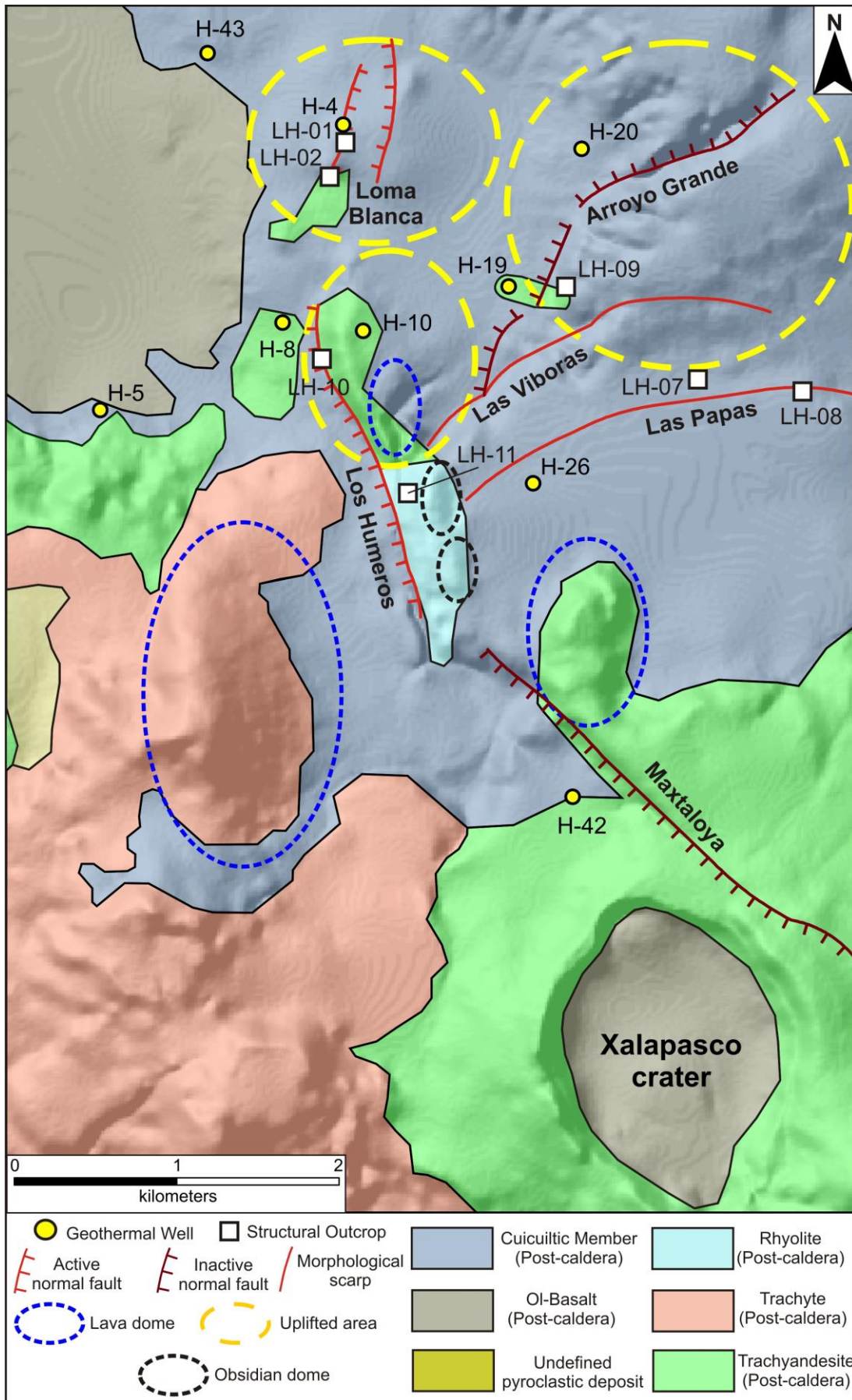
596

**Figure 2:** In depth correlation of lithostratigraphic units along the N-S (a) and W-E (b) direction (redrawn after Carrasco-Núñez et al. (2017a) and Arellano et al. (2003). Depth:horizontal distance=1:1. Location of the correlation line is shown in Figure 1. QigX= Xaltipan ignimbrite.



597  
 598  
 599  
 600  
 601  
 602  
 603  
 604  
 605  
 606  
 607  
 608  
 609  
 610  
 611  
 612  
 613  
 614  
 615  
 616  
 617  
 618  
 619  
 620

Figure 3: Experimental set-up. A motor controlled piston pushes upward the silicone at a fixed rate (2mm/hr) from the base of the layered sand pack (the diameter of the silicone is 8 cm). A laser scanner and a camera record the surface deformation induced by the intruding silicone.  $T$ = total overburden thickness.  $T_U$ = upper layer thickness,  $T_L$ = lower layer thickness.



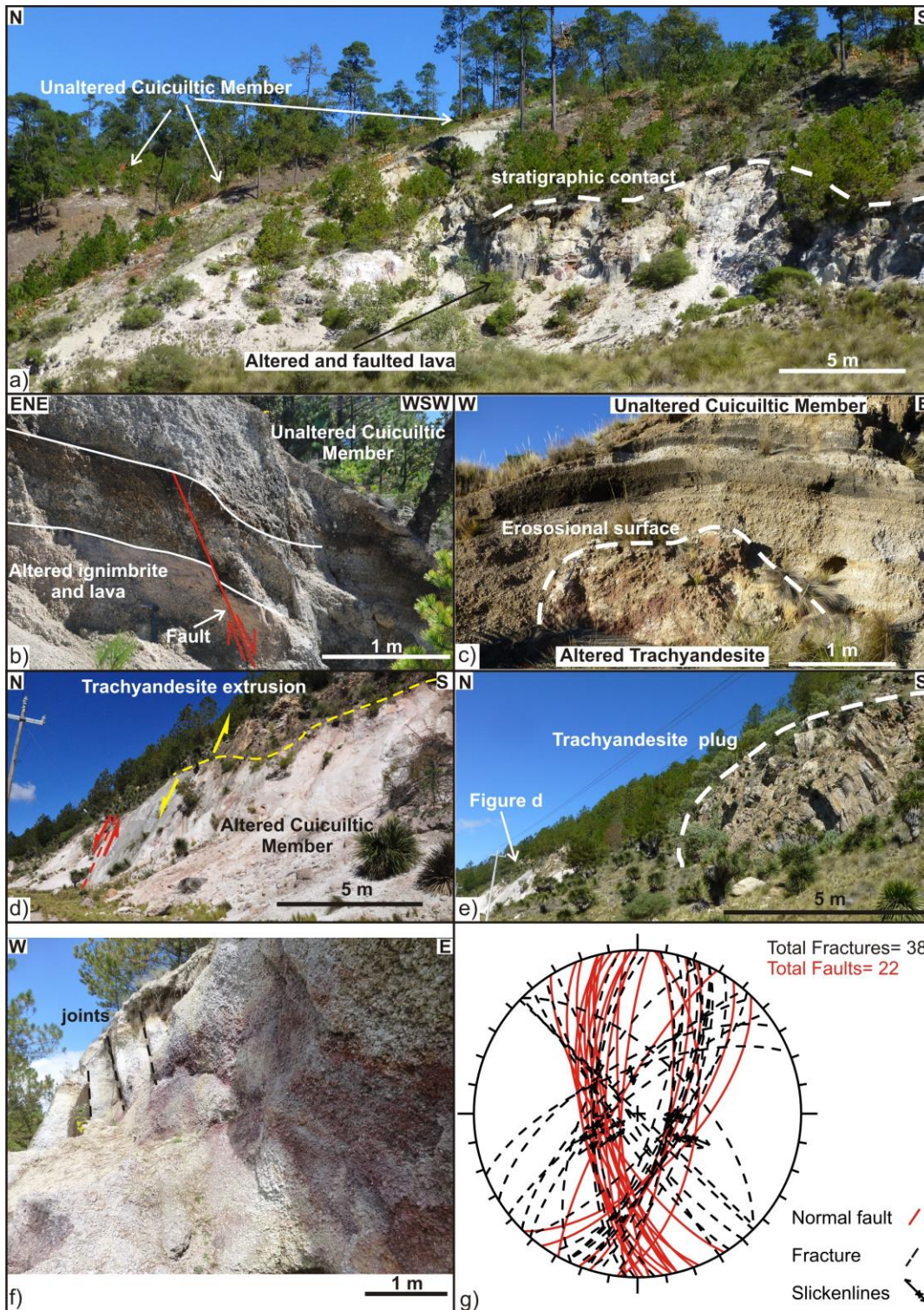
621  
622 **Figure 4: Simplified geological structural map of the studied area;reinterpreted after (Norini et al., 2015; Carrasco- Núñez et**  
623 **al., 2017b; Calcagno et al., 2018).**





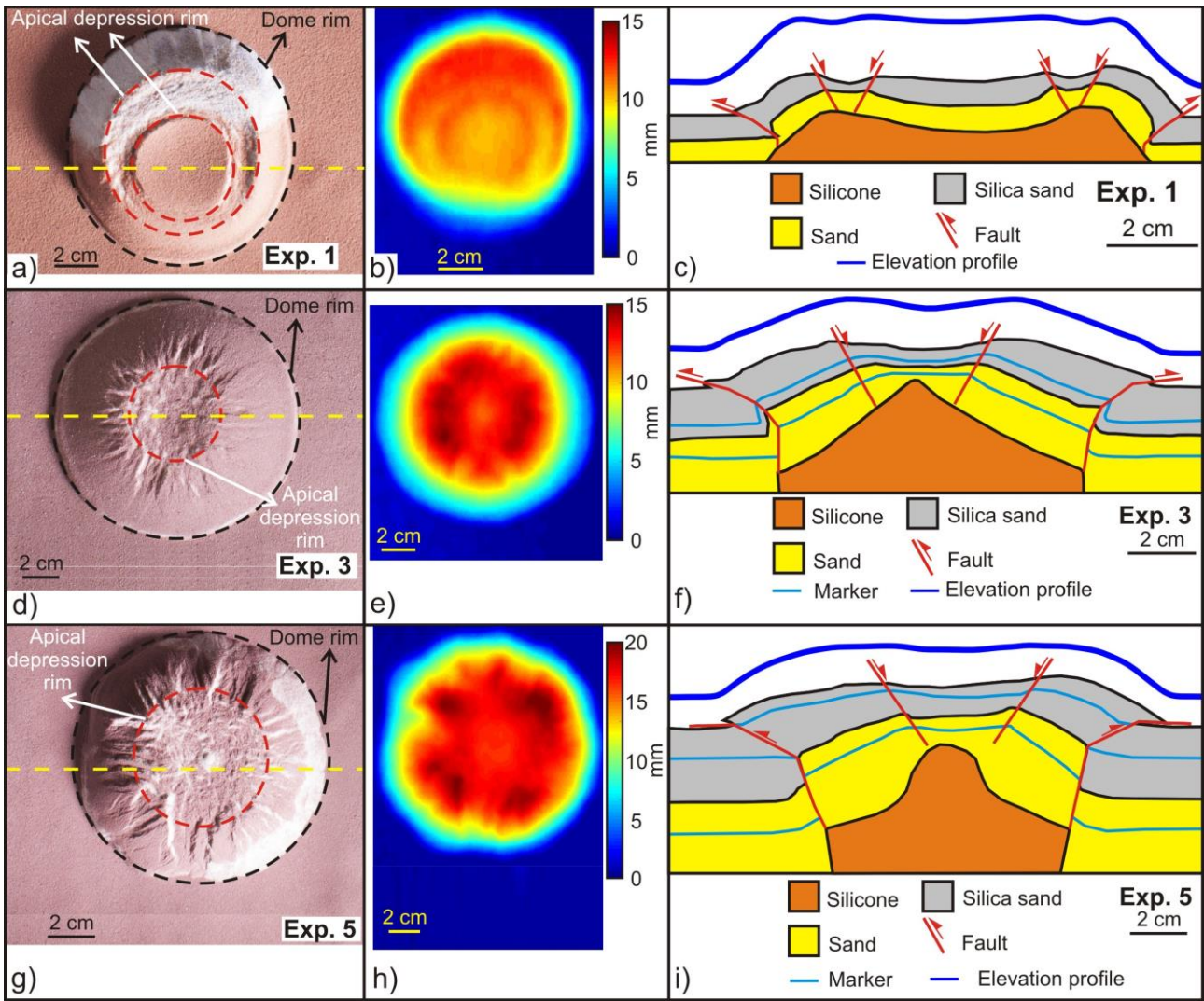
624  
 625 **Figure 5: a) Panoramic view from Xalapasco crater (looking towards N) of the lava domes aligned N-S. b) Unaltered**  
 626 **Cuicuiltic Member (LH-07). c) Unaltered Cuicuiltic Member covering a layered pyroclastic deposit, which can be laterally**  
 627 **correlated with the Xoxoctic Tuff (LH-08). The erosional surface preceding the deposition of the Cuicuiltic Member is shown**  
 628 **(dashed white line).**





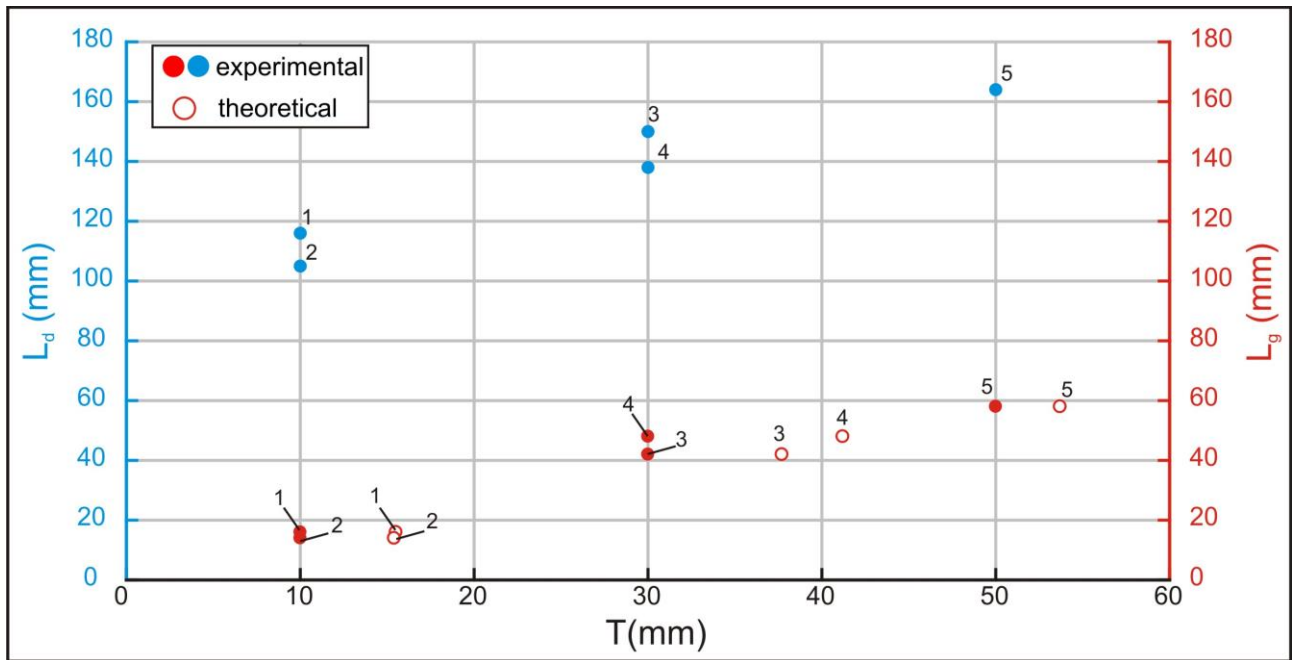
629  
 630 **Figure 6:** a) Panoramic view of the Arroyo Grande fault scarp showing the unaltered Cuicuiltic Member covering the altered  
 631 and faulted ignimbrite and lavas (site LH-09). b) Normal fault affecting the altered ignimbrite deposits unconformably  
 632 covered by the post-caldera, unaltered Cuicuiltic Member deposits (LH-09). Note that the Cuicuiltic Member deposits are  
 633 not faulted at this location; the fault can be thus considered as a fossil fault with respect to the Cuicuiltic Member deposition.  
 634 c) Block of altered trachyandesite buried by unaltered Cuicuiltic Member layers along the Maxtaloya fault scarp. d) Los  
 635 Humeros fault scarp (LH-10) induced by the ascent of the trachyandesitic extrusion on top of the fault plane. e)  
 636 Trachyandesite plug cropping out ~150 southward the fault scarp shown in d) (indicated by the red arrow). f) Jointing and  
 637 alteration of the Cuicuiltic Member within the apical depression of the Loma Blanca dome (LH-01). e) Equal-area stereo-plot  
 638 of the attitudes of faults and fractures in all the structural outcrops.





639  
640  
641  
642  
643  
644  
645  
646  
647  
648  
649  
650  
651  
652  
653  
654  
655  
656  
657

**Figure 7:** a) d) g) Top view image of the experiments 1, 3 and 5. b) e) h) cumulative vertical displacement; colour scale is proportional to the amount of uplift. c) f) i) Drawing of the cross section view obtained after cutting the section close to the dome center. The elevation profiles are obtained from laser scanner data. The yellow dashed line in a) d) g) indicates the trace of the section views and of the elevation profiles.

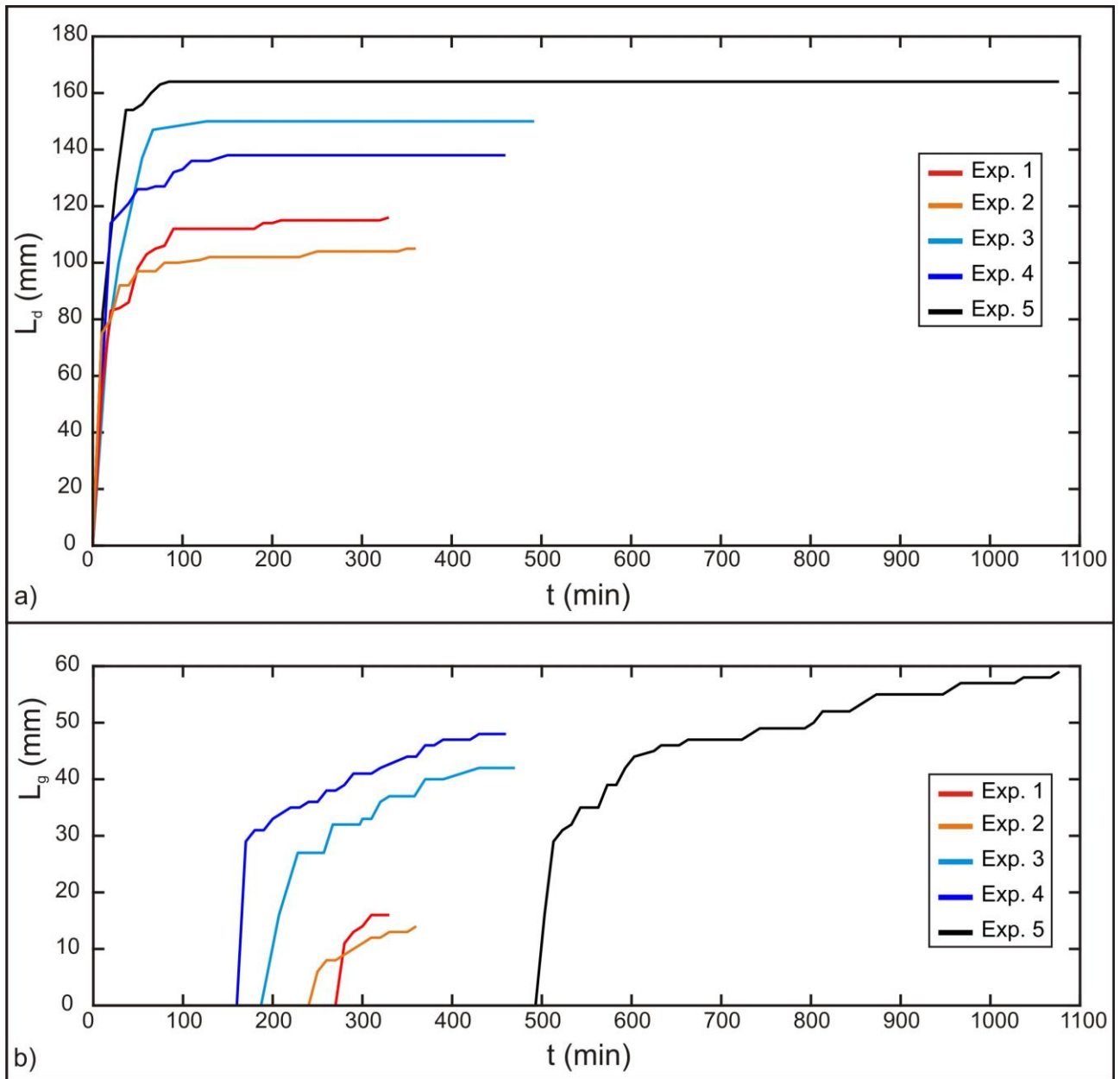


658

659

660

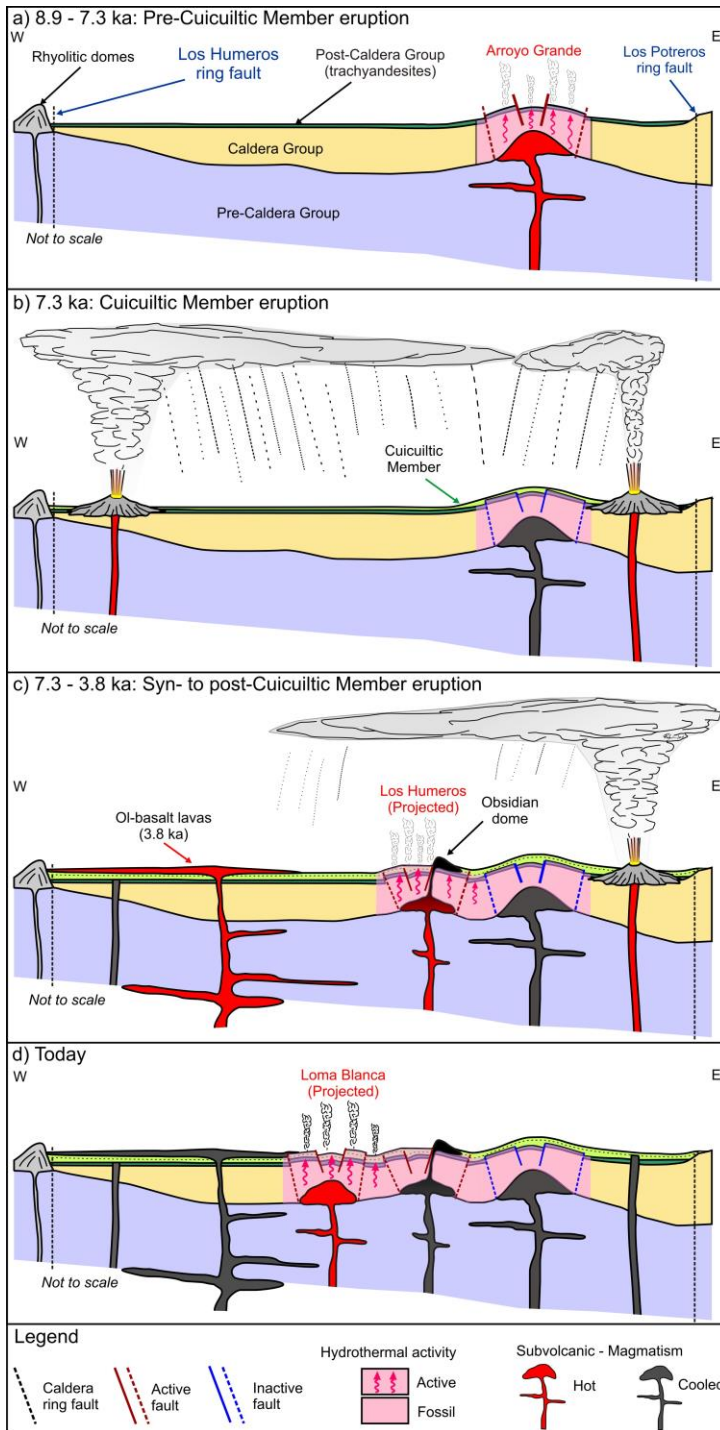
**Figure 8:  $L_g$  (apical depression width) and  $L_d$  (dome diameter) versus  $T$  (overburden thickness). Theoretical values calculated after equation 1 (see discussion section). The numbers above each point indicate the experiment number.**



661  
 662 **Figure 9: a) Time evolution of the dome diameter ( $L_d$ ). b) Time evolution of the apical depression width ( $L_g$ ). Both  $L_d$  and  $L_g$**   
 663 **show a similar evolution trend with a first stage of abrupt increase at the beginning of each experiment. In the second stage**  
 664  **$L_d$  becomes constant at  $t \sim 90$  min (experiments 1-2-3),  $t \sim 150$  min (experiment 4) and  $t \sim 65$  min (experiment 5) while  $L_g$**   
 665 **increases slightly from  $t \sim 250$ -280 min (experiments 1-2),  $t \sim 210$  min and  $\sim 170$  min (experiments 3 and 4) and  $t \sim 530$  min**  
 666 **(experiment 5) till the end of the experiment.**

667  
 668  
 669  
 670  
 671  
 672  
 673  
 674  
 675  
 676





677

678

679

680

681

682

683

684

685

686

687

688

**Figure 10: Schematic model of the evolution of the sub-surface structure of the Los Potreros caldera floor. Multiple magmatic intrusions located at relatively shallow depth (< 1 km) are responsible for the localized bulging of the caldera floor (Loma Blanca, Los Humeros and Arroyo Grande uplifted areas). a) Pre Cuicuiltic Member eruption: emplacement of a felsic intrusion at shallow depth and formation of the Arroyo grande bulge characterized by extensional faulting at its top, reverse faulting at its base and hydrothermalism. b) Cuicuiltic Member eruption: eruption of the Cuicuiltic Member covering the hydrothermally altered post-caldera trachyandesitic lavas. c) Syn to post Cuicuiltic Member eruption: formation of the Los Humeros fault and extrusion of obsidian lava domes along the fault scarp. As the trachyandesitic domes are covered with Cuicuiltic Member only at his base, the lava extrusion occurred during and post the Cuicuiltic Member eruption. d) Formation of the Loma Blanca bulge with the current hydrothermal activity and extensional faulting occurring within the apical depression. Notice that the emplacement of the successive most recent domes (Los Humeros and Loma blanca) are not aligned on the same plane, they are shown for practical purposes.**

Stage	Age (ka)	Main stratigraphic units
Post-caldera	< 69	Cuicuiltic Member and trachyandesitic to basaltic lavas
		Llano Tuff
		Xoxoctic Tuff
		Rhyolitic domes
Caldera	164-69	Zaragoza ignimbrite
		Faby Tuff
		Xaltipan ignimbrite
Pre-Caldera	700-164	Rhyolitic Domes

689 Table 1 Summary of the main stratigraphic units of the three evolutionary stages of the Los Humeros Volcanic complex  
690 (Carrasco-Núñez et al., 2017b, 2018).

Parameter	Definition	Value (experiments)	Value (nature)
T	Thickness of the overburden	1-5 X 10 <sup>-2</sup> m	300-2000 m
L <sub>d</sub>	Dome diameter	1-1.6 X 10 <sup>-1</sup> m	2000 m
H	Dome height	1.1-2 X 10 <sup>-2</sup> m	100 m
ρ <sub>s</sub>	Density of brittle overburden	1400 kg/m <sup>3</sup>	2800 kg/m <sup>3</sup>
φ	Angle of internal friction	35°	25-40°
τ <sub>0</sub>	Cohesion (brittle overburden)	300 Pa	10 <sup>6</sup> Pa
ρ <sub>m</sub>	Density of intrusive material	1000 kg/m <sup>3</sup>	2500 kg/m <sup>3</sup>
μ <sub>m</sub>	Viscosity of intrusive material	10 <sup>4</sup> Pa s	10 <sup>15</sup> Pa s
g	Gravity	9.8 m/s <sup>2</sup>	9.8 m/s <sup>2</sup>
t	Timespan for deformation	2.8-6.5 X 10 <sup>4</sup> s	1.9 X 10 <sup>12</sup> s

691 Table 2. Comparison of the geometric and material properties parameters of the experiments and nature.

Dimensionless ratio	Experiments	Nature
Π <sub>1</sub> = T/L <sub>d</sub>	0.1-0.5	0.15-1
Π <sub>2</sub> = H/L <sub>d</sub>	0.08-0.2	0.05-0.1
Π <sub>3</sub> = ρ <sub>s</sub> /ρ <sub>m</sub>	1.4	1.12
Π <sub>4</sub> = φ	35	25-40
Π <sub>5</sub> = ρ <sub>m</sub> H <sup>2</sup> /μ <sub>mt</sub>	6.1 X 10 <sup>-10</sup>	1.3 X 10 <sup>-20</sup>
Π <sub>6</sub> = ρ <sub>m</sub> gHt/μ <sub>m</sub>	1.3 X 10 <sup>3</sup>	4.6 X 10 <sup>3</sup>
Π <sub>7</sub> = ρ <sub>s</sub> gT/τ <sub>0</sub>	2.3	8.24

692 Table 3. Definition and values of the dimensionless ratios Π in nature and in the experiments.

Exp	T (mm)	L <sub>g</sub> (mm)	L <sub>d</sub> (mm)	θ	α	T <sub>t</sub> (mm)	σ (%)
1	10	16	116	58°	14°	15.5	55
2	10	14	105	63°	27°	15.4	54
3	30	42	150	58°	14°	37.7	27
4	30	48	138	56°	18°	41.2	37
5	50	58	164	58°	21°	53.7	7

693 Table 4. Measured (L<sub>g</sub>, L<sub>d</sub>, θ, α) and imposed (T) parameters in the experiments. T=overburden thickness; L<sub>d</sub>= dome  
694 diameter; L<sub>g</sub>= apical depression width; θ= apical depression fault dip; α= dome flank mean dip; T<sub>t</sub>= theoretical overburden

695 thickness calculated with equation 1 (Brothelände and Merle, 2015, see discussion section);  $\sigma$ = percentage difference between  
696 T and  $T_c$ .